universität
wien

DIPLOMARBEIT

Titel der Diplomarbeit

Numerical simulation and visualization of the Gross-Pitaevskii equation

zur Erlangung des Akademischen Grades

Magistra der Naturwissenschaften (Mag.rer.nat)

Verfasserin:	Sofi Esterhazy
Matrikel-Nummer:	A 0106175
Studienrichtung:	Mathematik
Betreuer:	Univ.-Prof. Dr. Norbert J. Mauser

Wien, November 2008

Acknowledgement

At this point I would like to thank all those people who supported me in realizing this work.

First of all I want to thank my supervisor Norbert J. Mauser for introducing me to this very interesting topic and making this work possible. I also want to thank the colleagues at the WPI, Hans-Peter Stimming for co-advising me e.g. in analysis of NLS and Harald Hofstätter for being my mentor in numerical applications.

Financial support of the WWTF (Wiener Wissenschafts-, Forschungs- und Technologiefonds) via the "Time Dependent Density Functional Theory" project (MA-45) of N. J. Mauser is gratefully acknowledged. In this context I want to thank Stefanie Preuss for her help in all administrative matters, too.

In addition, I really want to thank Thorsten Schumm from the AtomChip Group for all his support and his patience in helping Norbert J. Mauser to explain to me the relevant physics.

Finally I want to thank my friends for "keeping me in reality" and my whole family for believing in me and supporting me with so much love over all these years.

Abstract

This work presents the mathematical aspects of the modeling, analysis, simulation and visualization of Bose-Einstein condensates (BEC), a fascinating state of matter predicted by Einstein and Bose about 50 years before experimental realization has become a routine for quantum physicists.
In Vienna, mathematicians and physicists are effectively linked by the Wolfgang Pauli Institute (WPI) and in this environment it was very inspiring to work on this thesis. The idea was to work out really helpful visualizations of numerical simulations of the dynamics of BECs, thus helping the AtomChip Group to understand and design experiments.
In this mathematical thesis, of course, we also deal with the model equations and give an appropriate review of the corresponding analytical results as well as the practical aspects of numerics such as boundary conditions and implementation of algorithms. We concentrate mainly on the numerical simulation of the time-dependent system. We show, how the 3 different parts of the experiment: confinement, splitting and free expansion, are translated in three different mathematical challenges. Finally we present and discuss the methods which were used for the visualization.

This work is organized as follows:

Chapter 1 gives a short introduction in the state-of-the-art of physics and simulations of BEC.

Chapter 2 introduces some general analytical results of the Schrödinger equation. Well-posedness of the free Schrödinger equation (FSE), the cubic nonlinear Schrödinger equation (CNLSE) and the Gross-Pitaevskii equation (GPE) with different external potentials are discussed.

Chapter 3 describes the physical setup for the application on BECs. We give a formulation of the ground state problem and look in detail on the

time evolution of the condensate, where we distinguish between the confined regime, the splitting procedure and free expansion.

Chapter 4 deals with the numerical methods used for the simulation. First we present the imaginary time propagation (ITP) method for the ground state computation. Then, for the time-dependent system, we present the three different numerical schemes for the confined dynamics, the free expansion right after the switch-off of the trap, using the Strang-splitting-spectral (SSS) method in both cases, and free expansion neglecting of nonlinearity by evolving the FSE.

Chapter 5 documents the program package and the simulations of the WPI group. In addition, we give an extensive graphical representation of numerical results for all three dynamic regimes.

Zusammenfassung

Diese Arbeit behandelt die mathematischen Aspekte von Modellierung, Analysis, Simulation und Visualisierung des Bose-Einstein-Kondensats (BEC), eines faszinierenderen Zustands von Materie, den Bose und Einstein im Jahre 1924 vorhergesagt hatten, mehr als 50 Jahre bevor Quantenphysikern der experimentelle Nachweis gelang.
In Wien sind Mathematiker und Physiker im Wolfgang Pauli Institut direkt vernetzt, das daher ein sehr anregendes Umfeld fr die Arbeit an meiner Diplomarbeit bot. Das Ziel war, eine Visualisierung der numerischen Simulation der Dynamik von BECs auszuarbeiten und damit die AtomChip Gruppe darin zu unterstützten, Experimente zu verstehen bzw. neu zu konzipieren.
In dieser mathematischen Arbeit behandeln wir natürlich auch die Modellgleichungen und geben einen passenden Überblick sowohl über die entsprechenden analytischen Resultate also auch über die angewandten Aspekte der Numerik wie etwa Randbedingungen und Implementierung des Algorithmus. Wir konzentrieren uns hauptsächlich auf die numerische Simulation des zeitabhängigen Systems und zeigen, wie die drei verschiedenen Abschnitte des Experiments: Einsperrung, Aufspaltung und freie Ausbreitung, in drei verschiedene mathematische Problemstellungen übersetzt werden. Zum Schluss zeigen und diskutieren wir die Verfahren, die zur Visualisierung verwendet wurden.

Diese Arbeit ist wie folgt strukturiert:

Kapitel 1 zeigt in einer kurzen Einleitung die aktuellsten Erkenntnisse in der BEC-Physik und ihrer Simulation.

Kapitel 2 stellt allgemeine analytische Ergebnisse der Schrödingergleichung vor. Die Problemstellungen der Freien Schrödingergleichung (FSE), der kubischen nichtlinearen Schrödingergleichung (CNLSE) sowie der Gross-Pitaevskii Gleichung (GPE) mit unterschiedlichen externen Potentialen werden erörtert.

Kapitel 3 beschreibt den physikalischen Aufbau der mathematischen Gleichungen angewandt auf die Bose-Einstein-Kondensate. Wir formulieren das Problem des Grundzustands und untersuchen detailliert die Zeitentwicklung des Kondensats. Dabei unterscheiden wir zwischen den Abschnitten der Einsperrung, Aufspaltung und freien Ausbreitung.

Kapitel 4 handelt von den numerischen Methoden, die in der Simulation angewandt werden. Zuerst zeigen wir die Methode der imaginären Zeitpropagation für die Berechnung des Grundzustands. Im zeitabhängigen System unterscheiden wir die drei numerischen Methoden für die eingeschlossene Entwicklung, die freie Ausbreitung gleich nach dem Ausschalten der Falle, wobei in beiden Fällen die Strang-Splitting-Spectral-Methode angewandt wird, und die freie Ausbreitung unter Vernachlässigung der Nicht-Linearität, in der eine abgeänderte Methode der Fast-Fourier-Transformation (FFT) verwendet wird.

Kapitel 5 dokumentiert die Implementierung, die vom Wolfgang Pauli Institut angewandt wird. Zusätzlich zeigen wir eine ausführliche Darstellung der numerischen Ergebnisse für alle drei dynamischen Abschnitte.

Contents

Chapter 1

Introduction

The aim of this work is to give a comprehensive presentation of the full numerical simulation in three dimensions for the Bose-Einstein condensate (BEC). In cooperation with the AtomChip group[1] of Jörg Schmiedmayer on the Atom Institute of Austrian Universities, this is one of the current projects at the Wolfgang Pauli Institute[2] (WPI).

Aside from experimental realization of BECs with laser cooling and evaporation, different types of trapping potentials like magnetic or radio frequency traps have been extensively examined. After studying effects of dimension reduction, recent interest focuses on phenomena as vortices, coherent splitting or tunneling effects.

Scientists of the AtomChip group are specialized in realizing quasi-1d respectively quasi-2d atom traps as well as attaining tunnel-coupled wave packets. Unfortunately, the physical measurements only concedes restricted access to experimental data. Since the derivation of analytical solutions becomes way to elaborate, numerical computation is a very helpful and vital support.

Thus the intention of the work at the WPI was first to reproduce the physical dynamics of a BEC according to their experiments. Since the numerical results seem to be in good agreement with physical effects, a series of specified numerical simulation is planed in order to give predictions on future experimental applications of the AtomChip Group. The hope is to get a better understanding of the physics owing to the numerical results and possibly discover unpredicted new effects.

[1] http://www.atomchip.org
[2] http://www.wpi.ac.at

Over the years, an extensive analytical theory on the time dependent nonlinear Schrödinger equation was examined, but still some problems are not clarified. As a special case, the Gross-Pitaevskii equation represents the dynamics of a BEC and is one of the recent topics in the field of applied mathematics.

With physical methods it is only possible to do single snap-shots during the experiments, since the condensate is destroyed by the absorbing imaging method. Owing to these restrictive techniques of detection, a substantial request arose to find appropriate methods for the numerical simulation, assuring both reasonable accuracy as well as marginal computational effort.

Chapter 2

The Cauchy problem of the NLS

For many physical applications the general Schrödinger equation is one of the fundamental equations and contains a large class of partial differential equations.

We will concentrate on **time-dependent nonlinear Schrödinger equations** of the form

$$i\partial_t u = -\triangle u + V(x,t)u + f(u), \quad u = u(x,t), \quad x \in \mathbb{R}^n, t \in \mathbb{R}$$

$$u(x,t)|_{t=0} = u_I$$

where u is a complex function defined on $\mathbb{R}^{n+1}$, f is a nonlinear complex valued function and $V(x,t)$ a time-dependent external potential.
These equations apply to several physical phenomena and were generally studied in [19], [20] or [21].

2.1 On the free Schrödinger equation

Before looking at some particular classes of nonlinearity, we first study the free, linear Schrödinger equation

$$i\partial_t u(x,t) = -\frac{1}{2}\triangle_x u(x,t), \quad x \in \mathbb{R}^n, t \in \mathbb{R} \tag{2.1}$$

$$u(x,t)\Big|_{t=0} = u_I$$

We denote the time evolution operator group by $U(t) = e^{i\triangle\frac{t}{2}}$ such that the solution of (2.1) is of the form

$$u(x,t) = U(t)u_I(x) = e^{i\frac{\triangle}{2}t}u_I(x).$$

With Fourier transformation we can deduce a more explicit formula for the evaluation of $U(t)$. We have:

$$u(x,t) = \mathcal{F}^{-1}e^{-it\xi^2}\mathcal{F}u_I(x)$$

where $\mathcal{F}$ denotes the unitary Fourier transform with ξ as the transform variable, i.e.

$$\mathcal{F}f(x) = \hat{f}(\xi) = \int_{\mathbb{R}^n} f(x)e^{-2\pi ix\xi}dx$$

and $u_I \in \mathcal{S} = \{u \in C^\infty(\mathbb{R}^n) |\ \forall\alpha,\beta \in \mathbb{N}^n, \exists C_{\alpha,\beta} > 0, |x^\alpha\partial^\beta u(x)| \leq C_{\alpha,\beta},\ \forall x \in \mathbb{R}^n\}$.
Since $e^{-it\xi^2}$ is not in L^2, a more careful analysis is needed, but for $u \in L^1 \cap L^2$ it holds that

$$u(x,t) = \frac{1}{(4\pi it)^{n/2}}\int_{\mathbb{R}^n} e^{-i\frac{|x-\xi|^2}{4t}}\hat{u}_I(\xi)\ d\xi.$$

As the Fourier transformation satisfies the property $\mathcal{F}^{-1}\psi(x) = \mathcal{F}\psi(-x)$, a system described by the free Schrödinger equation is time reversible, i.e.: let $v = \overline{u(-t)}$, then v solves

$$-i\partial_t v = -\frac{1}{2}\triangle v, , \quad x \in \mathbb{R}^d, t \in \mathbb{R}$$

$$v(x,t)\Big|_{t=0} = \overline{u_I}$$

and $U(-t)\psi = \overline{U(t)\bar{\psi}}$.
Now let $u_I \in L^1$. Since $\mathcal{F}$ can get extended continuously to $L^1 \to L^\infty$ and the solution was denoted by

$$u(x,t) = \mathcal{F}^{-1}e^{-it|\xi|^2}\mathcal{F}u_I(x)$$

the evolution operator is continuous form $L^1 \to L^\infty$ and it holds:

$$\|u(x,t)\|_{L^\infty_x} \leq \frac{1}{(4\pi|t|)^{n/2}}\|u_I\|_{L^1_x}. \tag{2.2}$$

This inequality says that $u(x,t) = U(t)u_I(x)$ is bounded in such a way that the spatial supremum in the L^∞ sense, in dependence of time, is bounded

by the function $f(t) = c|t|^{-\alpha}, \alpha > 0$, which vanishes for $t \to \infty$ and thus is well-behaved in the $x \to \infty$ limit.

Likewise for $u_I \in L^2$ we have $U(t) : L^2 \to L^2$ and it holds

$$\|Uu_I\|_{L^2} = \|u_I\|_{L^2}, \tag{2.3}$$

since using the Plancherel theorem $\|u(x)\|^2_{L^2_x} = \|\hat{u}(\xi)\|^2_{L^2_\xi}$ gives

$$\begin{aligned} \|Uu_I\|^2_{L^2} &= \|\mathcal{F}^{-1}e^{-it\xi^2}\mathcal{F}u_I(x)\|^2_{L^2_x} = \|\mathcal{F}^{-1}(e^{-it\xi^2}\hat{u}_I(\xi))\|^2_{L^2_x} = \\ &= \|e^{-it\xi^2}\hat{u}_I(\xi))\|^2_{L^2_\xi} = \|\hat{u}_I(\xi)\|^2_{L^2_\xi} = \|u_I(x)\|^2_{L^2_x}. \end{aligned}$$

This is possible in the whole space $\Omega = \mathbb{R}^n$ and for appropriate (i.e. zero-Dirichlet) boundary conditions for a bounded Ω. In particular this equation describes the conservation of mass in quantum mechanics.

In general, for $u_I \in L^p$ and $p \in [2, \infty], t \neq 0$, the solution operator $U(t)$ is continuous from $L^p \to L^q$ with $\frac{1}{p} + \frac{1}{q} = 1$ and

$$\|U(t)u_I\|_{L^p} \leq \frac{1}{(4\pi|t|)^{\frac{n}{2}-\frac{n}{p}}}\|u_I\|_{L^q}$$

This inequality is called the dispersion estimate. It is an interpolation between (2.2), i.e. $p = \infty$, and (2.3), i.e. $p = 2$. If $u_I \in \mathcal{S}$, it can be proven for $2 < p < \infty$ by the Riesz-Thorin theorem, and by density arguments the statement for general u follows.

Related to the dispersive estimates is the classical Strichartz estimate for $u_I \in L^2$:

$$\|Uu_I\|_{L^{2+\frac{4}{n}}(\mathbb{R}^{n+1})} \leq C \ \|u_I\|_{L^2(\mathbb{R}^n)}$$

or more generally for $u_I \in L^2(\mathbb{R}^n)$ there exists a positive constant C such that

$$\|Uu_I\|_{L^q_t L^r_x(\mathbb{R}^n)} \leq C \ \|u_I\|_{L^2(\mathbb{R}^n)}$$

for an admissible pair (q, r), i.e. $q, r \in \mathbb{R}_+$ such that $q > 2$ and

$$\frac{q}{2} = \frac{n}{2} - \frac{n}{r} =: \delta(r)$$

and r must be in the range

$$2 \leq r < \frac{2n}{n-2} \text{ for } n \geq 3,$$

respectively $2 \leq r < \infty$ for $n = 2$ and $2 \leq r \leq \infty$ for $n = 1$. In particular, in the limit case $(q, r) = (\infty, 2)$ which is admissible for any dimension n, the inequality is consistent with the charge conservation (2.3). The end point case $(q, r) = (2, \frac{2n}{n-2}), n \geq 3$, has been a key tool for recent results in the study of nonlinear equations.
The general Strichartz estimate says that if the relation between space and time regularity of the solution $u(x, t)$ of (2.1) lies at the admissible line for the corresponding dimension, the function according to this norm can get bounded by the initial data in the L^2-norm. Thus from the property of admissible index pairs, one can see that the more the solution is regular in time the less it is regular in space and vice versa.

2.2 On the cubic Schrödinger equation

In the special case where we add a nonlinear term of the form $f(u) = \lambda|u|^2u$, the **cubic nonlinear Schrödinger equation (CNLSE)** appears owing to the two-particle collision interaction of a many-body quantum system. The according Cauchy problem can be written as:

$$i\partial_t u = -\triangle u + \lambda|u|^2u, \quad u = u(x,t), \quad x \in \mathbb{R}^n, t \in \mathbb{R} \tag{2.4}$$

$$u(x,t)|_{t=0} = u_I$$

where $\lambda \in R$ relates to the internal interaction. For $\lambda < 0$, we are in the focusing case which represents an attractive interparticle force; respectively $\lambda > 0$ is the defocusing case which represents a repulsive interparticle force. The Cauchy problem is locally well posed in $H^s(\mathbb{R}^n)$ for $s > \frac{n}{2} - 1$. In particular, on the so called energy space H^1 well-posedness holds for $n = 1, 2, 3$. But for $s = 0$, it fails for $n = 3$, is called the L^2-critical case for $n = 2$, and is well posed only for $n = 1$. Local existence can be proven by a Strichartz estimate and the Picard iteration scheme. Furthermore uniqueness of the solution follows by using the equivalent integral equation

$$u(x,t) = e^{it\triangle}u_I(x) - i\int_0^t e^{i(t-s)\triangle}\lambda|u(s)|^2u(s)ds$$

and a fix point argument such that $u \in C(\mathbb{R}, H_0^1(\Omega)) \cap L^q_{loc}(\mathbb{R}, L^\infty(\Omega))$ for every $q \in (2, 3)$.For $u_I \in H^1$ one uses the conservation of energy to control

the H^1-norm such that global existence holds.
We define the energy

$$E(u(x,t)) = \frac{1}{4}\|\nabla u\|_{L^2}^2 + \frac{\lambda}{2}\|u\|_{L^4}^4$$

and remember that energy conservation holds, i.e.

$$E(u(x,t)) \equiv E(u_I),$$

since multiplying equation (2.4) by $\overline{\partial_t u}$ and integration in x gives

$$-i\int \partial_t u\overline{\partial_t u}\,dx = \frac{1}{2}\int \triangle u\overline{\partial_t u}\,dx + \lambda\int |u|^2\overline{\partial_t u}\,dx$$

$$i\|\partial_t u\|_{L^2}^2 = \frac{1}{4}\partial_t\|\nabla u\|_{L^2}^2 + \frac{\lambda}{2}\partial_t\int |u|^4 dx = \partial_t E.$$

Thus we have $\partial_t E = 0$ since the real respectively imaginary part of both sides in the equation have to be equal. In the defocusing case, the H^1-norm can get bounded, since $||\nabla u||_{L^2}^2 \leq 4E(u_I)$ and in the focusing case, global well-posedness holds only for the one dimensional Cauchy problem. When global well-posedness fails, the solution can blow up after some finite time, i.e. $\exists T^* : \int |u|^2 \to \infty$ for $t \to T^*$. In particular this is the case when $\lambda < 0$ and $n \geq 2$. For more details on the single-power NLS see [22] ,[14] as well as [5].

2.3 On the Gross-Pitaevskii equation

In particular, we consider a class of cubic nonlinear Schrödinger equations with a further external potential known as the **Gross-Pitaevskii equation (GPE)**

$$i\partial_t u = -\triangle u + Vu + \lambda|u|^2 u, \quad u = u(x,t), \quad x \in \mathbb{R}^n, t \in \mathbb{R}$$
$$u(x,t)|_{t=0} = u_I$$

with $0 < \lambda \in \mathbb{R}$ and $V = V(x)$ being a confining real-valued potential $V : \mathbb{R}^n \to \mathbb{R}$.

The following two approaches can be pursued to study this equation.

On one side one could demand $V \in L^p$ and $p \geq 1, p \geq \frac{n}{2}$ to apply the theory of the CNLSE such that local existence and uniqueness are true. For the global result a further bound from below has to be imposed on V. With the known a-priori estimates on charge and energy, global existence can be proven.
On the other side one could use Kato's theory for the evolution operator of the linear problem. For this approach $V \in L^{\frac{n}{2}} + L^p$ has to hold such that the operator $-\frac{1}{2}\triangle + V(x)$ is self-adjoint. Then again techniques of the CNLSE can be used for the modified evolution operator instead of the free evolution operator, if they are not to "different" form each other.

If $V \in L^\infty + L^p$, for some $p \geq 1, p \geq n/2$, the Cauchy problem in $H^1(\mathbb{R}^n)$ is known to be locally well-posed, it may also lead to globally well-posedness or blow-up at finite time. If there is a smooth, non-negative potential $V \in C^\infty$with $D^\alpha V \in L^\infty$ for all $|\alpha| \geq 2$, the same holds in the domain of $\sqrt{\triangle + V}$. For more details, see R. Carles in [13] and references therein.

For the simplified potential $V \equiv -1$ initial data from the natural energy space $E = \{u \in H^1_{loc}(\Omega), \nabla u \in L^2(\Omega), |u|^2 - 1 \in L^2(\Omega)\}$ where $\Omega \subset \mathbb{R}^3$ is a compact subset, do not vanish at infinity. Therefore theory from GPE does not apply on $u_0 \in E \nsubseteq L^2(\Omega)$. Nevertheless uniqueness and local existence is in [5] shown such that $u \in C(R, E) \cap L^p_{loc}(R, L^\infty(\Omega))$ for every $q \in (2, 3)$. Moreover well-posedness holds on $\{u \in L^\infty, \nabla u \in L^2, |u|^2 - 1 \in L^2\})$ as well as global existence on E is shown by Zhidkov in [34]. This is extended to $d = 2, 3$ by Gerard [18] such that for $u_0 \in E$ and $p \in (2, 3)$ it holds that $u \in L^p([-T, T], L^\infty(\Omega))$, for some $T < 0$.

For an harmonic potential like $V = \frac{|x|^2}{2}$ the local problem can be treated as in the case with no potential by using the modified propagator for $-\frac{1}{2}\triangle + V$. If the initial mass and energy are defined at time $t = 0$, one can prove that the solution u is defined globally in time and the conservation of mass and energy hold, in the three dimensional case - especially with the commutative Heisenberg operators used in [12]. In detail, global well-posedness holds for $u_0 \in \Sigma := H^1(R^n) \cap \{u \in L^2(R^n), |x|u \in L^2(R^n)\}$, which is the corresponding energy space, and was studied by R. Carles in [11].

In the case of an anisotropic harmonic potential of the form $V = \frac{|x|^2}{2} + \frac{|z|^2}{2\varepsilon^4}$ with $x \in R^n, z \in R^d$ the problem can be simplified to lower dimension. First there has to be imposed a restriction to the nonlinearity in dependence to ε,

i.e. $\lambda = \varepsilon^d$, in order to conserve the homogeneity and the equation reads:

$$i\partial_t u = -\triangle_x u + \frac{|x|^2}{2}u + \frac{1}{\varepsilon^2}\big(-\triangle_z u + \frac{|z|^2}{2}u\big) + |u|^2 u$$

Then one has to apply a time scaling such that x, t are the slow variables of the same order and z the fast variable. In the limit $\varepsilon \to 0$ the nonlinearity and the x-component vanish and it remains a linear problem in z which can be solved exactly by spectral theory. With reinserting x, t and a projection on the ground state in the z-direction one gets an approximated solution:

$$u = \phi(x,t)e^{-i\mu_0 \frac{t}{\varepsilon^2}}\omega_0(z),$$

where (μ_0, ω_0) is the first pair of eigenvalue and eigenvector of the linear problem in z. Thus placing u into the full problem, it leaves to solve the reduced problem in ϕ:

$$i\partial_t \phi = -\triangle\phi + \frac{|x|^2}{2}\phi + \lambda_0|\phi|^2\phi \tag{2.5}$$

where $\lambda_0 = \lambda \int_{R^d} \omega_0^4(z)\, dz$. Finally it can be shown that the difference between the full solution and its approximation by (2.5) can be estimated by $\mathcal{O}(\varepsilon)$ and global existence of the original problem holds for $n + d < 4$ which includes the physically interesting case $n + d = 3$. For more details we refer to [1].

For a double-well potential like $V = \frac{1}{2}(x^2 - d)^2$ the Cauchy problem is globally well posed on H^1, if the parameter λ in the nonlinear therm is small enough. Moreover conservation of mass and energy are satisfied, too. In particular, the solutions have a special structure such that the problem can get approximated by a system of a two dimensional dynamical system that is exactly solvable. For more details see [30].

2.4 Finite computation domains and boundary conditions

Since in the computational context the whole space problem is always reduced to an approximation on a finite discretized domain, trivial boundary conditions like homogenous Dirichlet or periodic boundary conditions would invoke some unwanted dynamic effects. In particular this is the case for the

free flight modeling equations like CLNSE or FSE. In contrast, the wave packet won't leave the finite domain in the trapping regime modeled by the GPE with confining potential. Thus one has to impose further appropriate conditions on the artificially generated boundary.
There are two types of approaches to treat this. On one side one could think of inducing some absorbing boundary conditions in such a way that the solution at the boundary only contains outgoing waves. On the other side one could prescribe some damping behavior by an additional complex absorbing potential on an attached boundary layer of appropriate size. Here we will focus on the latter approach.

For the sake of a comprehensive notation, we consider the one-dimensional case ($n = 1$):
Let $[a, b]$ be the physically interesting interval on which the solution of the original Schrödinger equation is sought. Assuming the case where the initial data $u_0(x)$ is compactly supported on $[a, b]$, then one has to solve the following modified equation on the extended domain $[c, d]$:

$$i\frac{\partial}{\partial t}u(x,t) = (\mathcal{H} + V_C(x))u(x,t), \quad x \in [c,d], t > 0$$

$$u(x,0) = u_0(x), \quad x \in [c,d],$$

$$u(c,t) = u(d,t),\ u_x(c,t) = u_x(d,t), \quad t > 0$$

where $\mathcal{H}$ is the original Hamiltonian and the intervals $[c, a] \cup [b, d]$ are the locations of the absorbing boundary layers. The additional potential $V_C(x)$ is zero on $[a, b]$ and has a negative imaginary part on $[c, a] \cup [b, d]$, i.e.

$$V_C(x) = \begin{cases} -iW(x) & \text{on } [c,a] \cup [b,d] \\ 0 & \text{on } [a,b] \end{cases}$$

Therefore the modified equation reduces to the original NLS equations on [a, b] and plays the role of dampening the solution on $[c, a] \cup [b, d]$. If we focus on the left side of the boundary layer, the absorbing potential should be continuous and monotonic decreasing. In addition, it should satisfy $V_C'(a) = 0$. On the right side it should obviously satisfy similar conditions.
Unfortunately this leads to an effective non-hermitian Hamiltonian [29]. For that reason the choice of the complex potential function $V_C(x)$ becomes very essential. In particular, it has to avoid reflections back into $[a, b]$ as well as transmission resulting from the periodic boundary conditions.
For the linear Schrödinger equation the transmission and reflection coefficients of certain special imaginary potential functions can be analytically

obtained [25]. However for general imaginary potential functions these transmission and reflection coefficients need to be computed numerically. Here we present the particular choice of the imaginary potential function $V_C(x)$ being of the form of a polynomial of fifth order:

$$V_C(x) = \begin{cases} C_1(\frac{2(a-x)}{a-c})^5 & \text{on } [c,a] \\ 0 & \text{on } [a,b] \\ C_2(\frac{2(x-b)}{d-b})^5 & \text{on } [b,d] \end{cases}$$

where C_1, C_2 are constants which are numerically determined by the dominant wave number K and the boundary layer width $D = a - c = d - b$, in order to ensure a proper elimination of transmissions and reflections. In [33] they derived a full expression for the approximatively optimal coefficient, namely

$$C(K,D) = \min\left(22, \frac{880.42}{DK} + 1.0475\right)\frac{K^2}{100}.$$

With this method one can adaptively select the optimal absorbing potential with detecting K through a windowed Fourier transformation and thus it becomes a very convenient and reliable approach.

Chapter 3

Simulation of Bose-Einstein condensates

In the recent years physicists attained important and far reaching developments with experiments on dilute atomic Bose gases at zero or very low temperature. One of the most spectacular results in the field of atomic physics was the realization of quantum degeneracy below a critical temperature which lies in the nanokelvin range above absolute zero.
In 1924, Satyendra Bose and Albert Einstein already predicted that a system of trapped particles with integer spin called bosons should collapse into a single quantum ground state. But there had to pass another 70 years before the so called Bose-Einstein condensate (BEC) was realized, in 1995, independently by research groups on the JILA and MIT [16, 4].

Over the years, physicists were seeking to improve different trapping techniques and cooling procedures. First, in the experimental setups current carrying wires were situated outside a vacuum chamber in order to produce BEC at ultra cold temperature. In consequence, large electric current rates were necessary which caused high power consumption and heat dissipation. Thus the idea came up to bring the field generating structures inside the vacuum chamber and reduce the wire size to increase the current density, at the same time. This leads to the invention of atom chips with which creation of BEC was realized successfully for the first time in 2001 [23, 28].

3.1 Experimental realization of BEC

Bose-Einstein condensation occurs when the thermal deBroglie wavelength $l_B = \hbar/mv_t$, where v_t is the atom's thermal speed and m the atomic mass, becomes larger than the mean interparticle separation length. This can only happen at extremely low temperature such that a macroscopic number of atoms start to occupy the same quantum ground state of the external potential. Then the atomic wave packets overlap (forming a giant matter wave [32]), behaving as a single quantum entity.

The experimental setup starts with activating a magneto-optical trap (MOT) which consists of a magnetic quadrupole field supplied by a static magnetic field, generated by U-shaped copper-wire structure underneath the chip, and a homogeneous bias field backed with a six-beam laser configuration which overlaps in the trapping region.

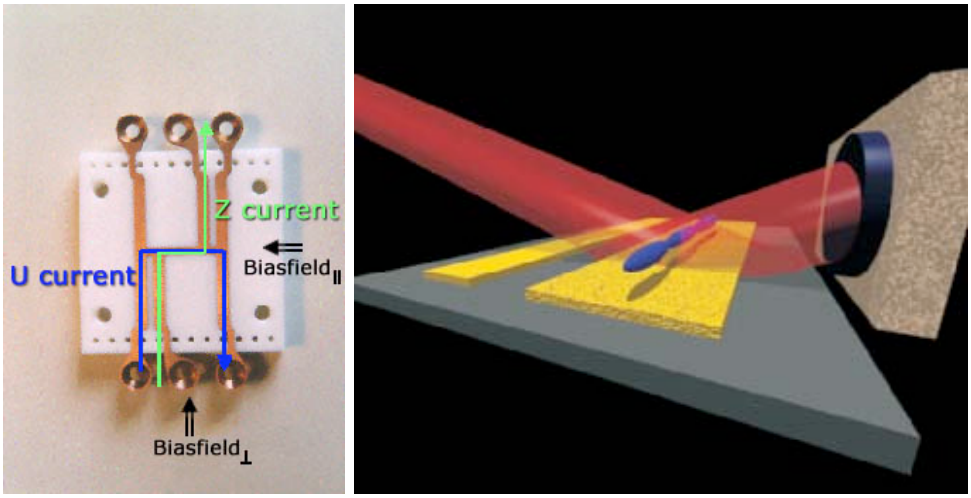

Figure 3.1: Left: Photograph of the macroscopic wire structures mounted underneath the atom chip. Right: Simulation of the experimental set-up. A Bose-Einstein condensate (blue) is created and trapped by a current-carrying wire (gold) mounted on the silicon surface of the atom chip (grey). The laser beam (red) from a CCD camera indicates the imaging assembly. Allocated by the AtomChip Group.

Afterwards the quadrupole field is turned off while the cooling is proceeded in an intensifying way in optical molasses. Next, a small bias field is turned on to provide the final optical pumping, where they are transferred to the desired spin-state for purely magnetic trapping.

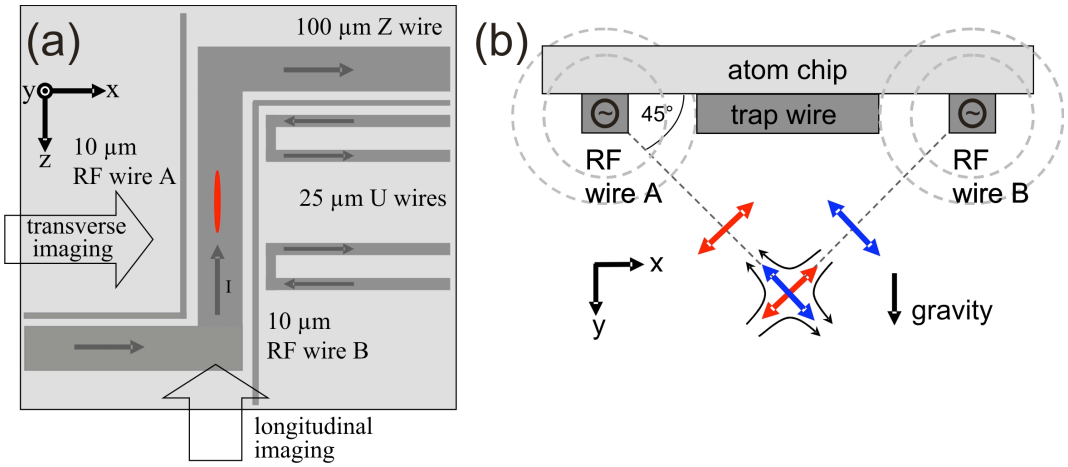

Figure 3.2: Schematic of the three-wire rf trap (a) top view, (b) side view from the longitudinal direction. Allocated by the AtomChip Group.

Then a purely magnetic trap is turned on, using a Copper Z-trap together with a homogeneous field, parallel to the wire plane, which creates a Ioffe-Pritchard type trap, and synchronized with the optical molasses. At this stage a first evaporative cooling is established. After that the Z-trap is delicately "replaced" by the traps generated with wires on the atom chip. Finally a second radio frequency cooling (rf) cooling is applied to ensure that the atoms are captured in the ground state of the trap. A very detailed description of this process is explained in the PhD thesis of S. Hofferberth [24].
This is the moment where usually mathematical modeling sets off.

3.2 The ground state problem

For the sake of completeness we give a short review on the formulation of the minimal energy state problem. In physics, it was an expensive and elaborate procedure to accomplish temperature near absolute zero such that almost all particles get into the ground state. By contrast, mathematics is dealing with the idealized situation where particles occupy all the same state. However finding the analytical solution turns out to be a complex procedure as well.

The ground state is considered to be of the stationary form

$$u(\mathbf{x}, t) = e^{-i\mu_0 t}\phi_0(\mathbf{x})$$

where $\phi_0(\mathbf{x})$ is the corresponding eigenfunction to the minimal eigenvalue μ_0 of the following nonlinear eigenproblem

$$\mu\phi(\mathbf{x}) = -\frac{1}{2}\triangle\phi(\mathbf{x}) + V(\mathbf{x})\phi(\mathbf{x}) + \lambda|\phi(\mathbf{x})|^2\phi(\mathbf{x})$$

under the constraint

$$\int |\phi(\mathbf{x})|^2 \, d\mathbf{x} = N.$$

Besides, the ground state can also be defined as the solution of the minimization problem $E(\phi_0) = \min_{||\phi||^2=1} E(\phi)$ of the energy functional

$$E(\phi) = \int_{R^d} \Big[\frac{1}{2}|\nabla\phi|^2 + V|\phi|^2 + \frac{\lambda}{2}|\phi|^4\Big] d\mathbf{x}$$

and the corresponding eigenvalue can be computed by the relation

$$\mu(\phi) = E(\phi) + \frac{\lambda}{2}\int |\phi|^4 d\mathbf{x}$$

such that $\mu_0 = \mu(\phi_0)$ can be seen as the chemical potential of the condensate.

Further properties of the functional as well as properties of the functional conditions for existence and uniqueness of the minimizer were concisely summarized in the paper of Bao et al. [7]:

"The energy functional is positive, coercive and weakly lower semicontinuous on the unit sphere in $L^2(\mathbb{R}^3)$, thus the existence of a minimum follows from standard theory. For understanding the uniqueness question note that $E(\alpha\phi_0) = E(\phi_0)$ for all $\alpha \in C$ with $|\alpha| = 0$. Thus an additional constraint has to be introduced to show uniqueness, e.g., ϕ_0 real valued and $E(\psi)$ is not bounded from below on the unit sphere of $L^2(\mathbb{R}^3)$. Thus, an absolute minimum of $E(\psi)$ does not exist on $\{\psi \in L^2(\mathbb{R}^3)|\|\psi\|^2 = 1\}$. The interpretation of critical points (local min., saddle points) as physically relevant ground states is by no means clear."

3.3 Dynamics of BECs

After realizing the cooling procedure, physicists continued doing experiments by manipulating the external potential and then releasing the atoms to free expansion.

3.3.1 Trapped condensate

In order to induce BEC, particles have to be confined in a magnetic trap which can be represented by an axially symmetric, three dimensional harmonic potential. Further on physicists started to generate traps of very anisotropic form, reaching the limit of quasi-two dimensional and quasi-one dimensional systems, such that interesting effects of reduced dimensionality can be investigated as well.
The according mathematical system can be described by the following GPE in physical units:

$$i\hbar\frac{\partial u(\mathbf{x},t)}{\partial t} = -\frac{\hbar^2}{2m}\triangle u((\mathbf{x},t) + V((\mathbf{x})u((\mathbf{x},t) + N\frac{4\pi\hbar^2 a}{m}|u((\mathbf{x},t)|^2 u((\mathbf{x},t)$$

where $\hbar$ is the Planck constant, N the number of atoms in the condensate, m the atomic mass, a the s-wave scattering length and $V(x)$ is an external trapping potential. In addition, we require the condensate wave function u to be normalized to the number of atoms, i.e.

$$\int |u|^2 d\mathbf{x} = N.$$

As it was already described by Bao et al. in [9] we list two special examples for trapping potentials which were exploited by physicians in the last years:

First we present the classical 3D harmonic oscillator potential:

$$V_{ho}(\mathbf{x}) = \frac{m}{2}\omega^2\mathbf{x}^2 = \frac{m}{2}(\omega_x^2 x^2 + \omega_y^2 y^2 + \omega_z^2 z^2)$$

where ω_x, ω_y and ω_z are the trap frequencies in the x-, y- and z-direction respectively.

And as a further example we give a 2D harmonic oscillator with a 1D double-well potential:

$$V_{dw}(\mathbf{x}) = \frac{m}{2}(\omega_x^2(x^2 - d)^2 + \omega_y^2 y^2 + \omega_z^2 z^2)$$

where d is the distance between the double-well minima.

For both potentials one can choose $\omega_x = \omega_y = \omega_\perp \ll \omega_z$, which gives one respectively two disc-shaped traps, or $\omega_\perp \gg \omega_z$ for one respectively two

cigar-shaped traps.

Furthermore, in both examples, we can give the scaling transformation

$$\tilde{t} = \frac{t}{t_0}, \tilde{\mathbf{x}} = \frac{\mathbf{x}}{x_0}, \text{and } \tilde{u}(\mathbf{x}, t) = \mathbf{x}_0^{3/2} u(\mathbf{x}, t)$$

where the scaling parameters of dimensionless time respectively length units t_0, x_0 have to be chosen in an appropriate form to the external potential, i.e.:

$$t_0 = \frac{1}{\omega_x}, \mathbf{x}_0 = \sqrt{\frac{\hbar}{m\omega_x}} \text{ respectively } d_s = \frac{d}{\mathbf{x}_0}.$$

Plugging this transformations into the GPE, multiplying by $t_0^2/m\mathbf{x}_0^{1/2}$, and then omit all $\tilde{}$, we obtain the following dimensionless GPE under the normalization condition in three dimensions:

$$i\frac{\partial u(\mathbf{x}, t)}{\partial t} = -\frac{1}{2}\triangle u(\mathbf{x}, t) + V(\mathbf{x})u(\mathbf{x}, t) + \beta N \frac{4\pi a}{\mathbf{x}_0}|u(\mathbf{x}, t)|^2 u(\mathbf{x}, t)$$

with the dimensionless parameter $\beta = 4N\pi a/\mathbf{x}_0$ and $V(\mathbf{x}) = \frac{1}{2}(x^2 + \frac{\omega_y}{\omega_x}y^2 + \frac{\omega_z}{\omega_x}z^2)$ respectively $V(\mathbf{x}) = \frac{1}{2}((x^2 - d_s^2)^2 + \frac{\omega_y}{\omega_x}y^2 + \frac{\omega_z}{\omega_x}z^2)$.

3.3.2 Splitting the condensate

Incidentally, one of the main interests is to achieve coherent control over Bose-Einstein condensates in order to realize a kind of a miniaturized matter wave interferometer. Therefore the confining trap of the BEC is dynamically changed from a single minimum to a double well configuration, which separates a single initial condensate into two parts. But it is imperative that the split procedure maintains the phase coherence (is phase preserving, in analogy to a beam splitter in optics).

This system can again be modeled by the GPE, where the external potential is now time-dependent:

$$i\hbar\frac{\partial u(\mathbf{x}, t)}{\partial t} = -\frac{\hbar^2}{2m}\triangle u(\mathbf{x}, t) + V(\mathbf{x}, t)u(\mathbf{x}, t) + N\frac{4\pi\hbar^2 a}{m}|u(\mathbf{x}, t)|^2 u(\mathbf{x}, t)$$

As it is described in detail in [24], the effective adiabatic potential is constituted by two magnetic fields. One is a static magnetic field, created by the Z-trap in the x-y plane which can be approximated by

$$\mathbf{B}_{\mathrm{S}}(\mathbf{x}) = G\rho[\cos\psi\mathbf{e}_x - \sin\psi\mathbf{e}_y] + B_I\mathbf{e}_z$$

where G is the gradient of a quadrupole field perpendicular to the central part of the Z-wire, B_I the constant amplitude of a parallel Ioffe field, $\rho = \sqrt{x^2 + y^2}$ and $\psi = \arctan \frac{y}{x}$ the polar coordinates.
The other is a radio frequency (rf) field being a superposition of two perpendicular, linear fields, produced by the two rf wires parallel to the middle part of the Z-wire (see figure), such that

$$\mathbf{B}_{\mathrm{rf}}(\mathbf{x})e^{\omega_{\mathrm{rf}}t} = \Big[B_{\mathrm{A}}(t)\mathbf{e}_x + B_{\mathrm{B}}(t)e^{i\delta}\mathbf{e}_y\Big]e^{\omega_{\mathrm{rf}}t}$$

with δ a phase shift between the two components of the rf field in order to balance the antisymmetric structure on the atom chip. This oscillating field induces the splitting process by increasing the current in both rf wires.

Incidentally, the measures of the rectangular shaped wires are expected to be known such that the according magnetic field of rectangular shaped wires is given by (Biot-Savart law)

$$\mathbf{B}(\mathbf{x}) = \int_{-W/2}^{W/2}\int_{-H/2}^{H/2}\int_{-L/2}^{L/2} \frac{\mu}{4\pi}\frac{\mathbf{j}\times(\mathbf{x}-\mathbf{x}')}{|\mathbf{x}-\mathbf{x}'|^3}d\mathbf{x}'$$

where W, H and L are the width, height and length of the wire and $\mathbf{j} = \frac{I(t)}{WH}\mathbf{e}_z$ is the current density. We have a constant current, i.e. $I(t) \equiv I_S$ for the static field and a linear increasement of the current for the rf field, i.e. $I(t) = c\frac{t}{t^*}$ and $[0, t^*]$ the time interval of the splitting procedure.

With a unitary transformation to the magnetic field operators such that the interaction of the atoms with $|\mathbf{B}_{\mathrm{S}}(\mathbf{x})|$ is diagonal, and a further operation which leads to a so-called rotating wave approximation, as it is presented by I. Lesanovsky et al. [26], one can neglect the fast time scale oscillating term and the potential transforms to

$$V_{ad} = \tilde{m}_F g_F \mu_B \sqrt{\triangle(\mathbf{x})^2 + \Omega(\mathbf{x},t)^2}$$

where $\tilde{m}_F$ is the according quantum number, g_F the Landé factor corresponding to the total angular momentum of the atom, μ_B the Bohr magneton, with the detuning and the Rabi frequency defined by

$$\triangle(\mathbf{x}) = |\mathbf{B}_{\mathrm{S}}(\mathbf{x})| - \frac{\hbar\omega}{g_F\mu_B}$$

$$\Omega(\mathbf{x},t) = \frac{1}{2}\sqrt{\frac{B_A(t)^2 + B_B(t)^2}{|B_S(\mathbf{x})|^2}\Big(B_I^2 + G^2\rho^2 f(\psi)\Big)}$$

with $f(\psi) = (1 - \cos(2\alpha)\cos(2\psi) \pm \sin(2\alpha)\sin(2\psi))/2$ and $\tan(\alpha) = \frac{B_B}{B_A}$.

In practice, the time-dependent potential is explicitly given by an analytical expression for each time step. This means that one calculates with a new Hamiltonian after each iteration step.

3.3.3 Free expansion

As long as the atom cloud is controlled by a confining potential, the typical behavior from the condensate can not be monitored using absorbing imaging. Thus, generating a sudden switch-off of the trapping potential at a particular time $t = t^*$, expansion of the condensate can be observed by a time-of-flight measurement.

Thus we can assume $V(\mathbf{x}, t) \equiv 0$ for $t > t^*$ such that the propagation can be described by the CNLSE with physical units:

$$i\hbar\frac{\partial u(\mathbf{x},t)}{\partial t} = -\frac{\hbar^2}{2m}\triangle u(\mathbf{x},t) + N\frac{4\pi\hbar^2 a}{m}|u(\mathbf{x},t)|^2 u(\mathbf{x},t), \quad \mathbf{x} \in \mathbb{R}^3, t > t^*.$$

In particular, after some time of spreading, particle interaction becomes negligible such that we can drop the nonlinear term. Thus it is sufficient to describe time evolution by the free Schrödinger equation for $t^{**} > t^*$:

$$i\hbar\frac{\partial u(\mathbf{x},t)}{\partial t} = -\frac{\hbar^2}{2m}\triangle u(\mathbf{x},t), \quad \mathbf{x} \in \mathbb{R}^3, t > t^{**}$$

Here the equation can easily be rescaled to a dimensionless formulation by

$$\tilde{\mathbf{x}} = \frac{\mathbf{x}}{\mathbf{x}_0}, \text{and } \tilde{t} = \frac{\mathbf{x}_0^2\, m}{\hbar}t$$

where $\mathbf{x}_0$ is the intrinsic length unit such that by multiplying with $\hbar^2/(\mathbf{x}_0^2\, m)$ and leaving all $\tilde{}$, we get the simplified form:

$$i\frac{\partial u(\mathbf{x},t)}{\partial t} = -\frac{1}{2}\triangle u(\mathbf{x},t)$$

Chapter 4

Numerical methods

The computational simulation starts with solving the ground state problem. Afterwards we distinguish, within the time propagation of the system, between the confined dynamics and the free expansion of the condensate.

4.1 Discretization

For the numerical setup we first introduce a discretization in three dimensional space. Therefore we choose some values $x_{min}, x_{max}, y_{min}, y_{max}, z_{min}, z_{max}$ sufficiently large which determine the computational domain $\Omega = [x_{min}, x_{max}] \times [y_{min}, y_{max}] \times [z_{min}, z_{max}]$. Then we fix the numbers of discretization steps n_x, n_y, n_z which defines the discretization mesh sizes in three dimensions

$$\triangle x = \frac{x_{max} - x_{min}}{n_x},\ \triangle y = \frac{y_{max} - y_{min}}{n_y},\ \triangle z = \frac{z_{max} - z_{min}}{n_z}$$

Additionally we have to choose a time discretization step size $\triangle t$ and an end time $T > 0$ for the time propagation on the interval $[0, T]$.

Accordingly we will work on the equidistant grid points

$$\begin{aligned} x_j &:= x_{min} + j\triangle x, \quad j = 0, \ldots, n_x - 1 \\ y_k &:= y_{min} + k\triangle y, \quad k = 0, \ldots, n_y - 1 \\ z_l &:= z_{min} + l\triangle z, \quad l = 0, \ldots, n_z - 1. \end{aligned}$$

and

$$t_n := n \cdot \triangle t,\ n = 0, \ldots, \frac{T}{\triangle t} = N.$$

For simplicity of notation we will illustrate the numerical schemes in one space dimension ($d = 1$) only. The generalization to higher dimensional problems is straight forward.

Hence we define some values x_{min}, x_{max} determing the computational domain $\Omega = [x_{min}, x_{max}]$ and fix the number of discretization points n_x for the spacial mesh size

$$\triangle x = \frac{x_{max} - x_{min}}{n_x}.$$

Thus we get the grid points

$$x_j := x_{min} + j\triangle x, \quad j = 0, \ldots, n_x - 1$$

$$t_n := n \cdot \triangle t, \ n = 0, \ldots, \frac{T}{\triangle t} = N.$$

Further on we will abbreviate $u(x_j, t_n)$ by u_j^n. Likewise we will denote the solution vector at time $t = t_n$by $u^n = (u_j^n)_{j=0,\ldots,n_x}$

4.2 Computation of the ground state

Since the dynamics of BEC act in a very sensitive way due to initial data, it is important to compute the ground state with sufficient accuracy. According to the analytical setup one could think to use a numerical eigenvalue or variational solver in order to compute the ground state of the GPE. There exist several effective methods to diagonalize the Hamiltonian for the linear case. Owing to the appearance of the nonlinearity this expands to a sequence of linearized problems that has to be solved iteratively. Consequently, it requires an extensive computational cost.
Thus one could think of using some dynamic procedures. In the past, different techniques have been developed. A Runge-Kutta method was studied by Burnett et al. [17] or a direct scheme of minimizing $E(\phi)$ by a finite elements method (FEM) was examined by Bao et al. [10] as well as the normalized gradient flow method in [6].

A common method to compute the ground state is imaginary time propagation (ITP) of the Schrödinger equation. By the transformation $t \to \tau = -it$

the problem turns into a diffusion system

$$\partial_\tau v = -Hv, \quad \text{where } H = \frac{\hbar}{2m}\nabla^2 + V(x) + \lambda|v|^2.$$

This equation can be solved by an appropriate numerical scheme similar to the method presented in the next section.
Starting with an arbitrary initial data v_0 for $\tau = 0$ satisfying $\|v_0\|_{L^2_x} = 1$, the solution $v(x,\tau)$ usually converges quickly towards the ground state $\psi_0(x)$ for $\tau \to \infty$, while $\|v(x,\tau)\|_{L^2_x} \leq \|v(x,\tau_n)\|_{L^2_x} = 1$ for $\tau_n \leq \tau \leq \tau_{n+1}, n \geq 0$. Therefore the solution hast to be normalized after each time step in order to guarantee... Furthermore, we have

$$E(v(x,\tau)) \leq E(v(x,\tau')) \quad \text{for } \tau_n \leq \tau' \leq \tau \leq \tau_{n+1}, n \geq 0.$$

This inequality is called the energy diminishing property of the gradient flow, see [6] . With similar arguments used for the Ginzburg-Landau models [27, 31], describing phenomena for superconductivity in isotropic, homogeneous material samples, we get that v approaches the ground state solution as $\tau \to \infty$.

For the or numerical computation, one has to determine a suitable break-off condition. As a criterion for convergence we use an upper bound $\varepsilon \ll E = \langle v|H|v\rangle$ for the standard deviation of the energy such that

$$\triangle E = \sqrt{\langle u|H^2|u\rangle - \langle u|H|u\rangle^2} < \varepsilon.$$

4.3 Time propagation

For the numerical study of the time evolution problem many approaches were pursued and adapted in order to achieve better computational results. Over the years, numerous numerical methods for the time dependent solution of the GPE were investigated.
One of the suitable methods is the the unconditionally stable, implicit Crank-Nicholson finite-difference method (CNFD) [2], [8] which conserves the basic properties like mass conservation as well as energy conservation, but no time transverse invariance. This scheme has accuracy of 2nd order in both, space and time. The explicit Leap-Frog finite-difference method (LPFD) [15] only

conserves energy and is time reversible, but still temporal and spacial accuracy is of 2nd order. The stability here is limited by the discretization steps, i.e. $\triangle t(|4/(\triangle x)^2 + V_{max}|) < 2$ which does not affect the CFL condition $\triangle t \sim (\triangle x)^2$. A more convenient approach would be the implicit Crank-Nicholson pseudo-spectral method (CNSP) vgl. [8] where conservation of mass and energy are served, it is time reversible, unconditionally stable, of spectral accuracy in space and 2nd order in time. Only time transverse invariance and dispersion relation fail. Beside, Adhikari was studying a Runge-Kutta pseudo-spectral method of forth order (RKSP4) [3] which is of spectral accuracy in space, but even time reversibility is not satisfied.

4.3.1 Confined Dynamics

After the ground state procedure, we initialize the real time simulation with the resulting self-consistent wave function.

First we discuss the system modeled by the GPE with a **time independent external potential** $V(x)$.

$$i\hbar\frac{\partial}{\partial t}u(x,t) = -\frac{\hbar^2}{2m}\nabla^2 u(x,t) + V(x)u(x,t) + \lambda|u(x,t)|^2 u(x,t).$$

We assume that this system is valid for $t \in [0, T_1]$.

Here we will present in detail a time splitting spectral (TSSP) method. The idea is to split the operator $H = H_0 + W$ into the kinetic part

$$H_0 = -\frac{\hbar^2}{2m}\triangle_x$$

and the potential part

$$W = V(x) + \lambda|u|^2$$

because for each separate part, the time propagation can be solved exactly.

For the time propagation of the **kinetic part**

$$i\partial_t u = -\frac{\hbar}{2m}\nabla^2 u$$

the formal solution is

$$u^1 = \mathcal{F}^{-1} e^{-i\hbar\triangle t p^2/2m}\mathcal{F}u^0$$

where $\mathcal{F}$ denotes the continuous Fourier transform. For the discretization in space this translates into

$$u_j^1 = \frac{1}{n_x} \sum_{k=-n_x/2}^{n_x/2-1} e^{-i\hbar(\frac{2\pi k}{L})^2 \triangle t/2m} \hat{u}_k^0 e^{i\frac{2\pi k}{L}(x_j - x_{min})}$$

where $L = x_{max} - x_{min}$ and $\hat{u}_k^0 = \sum_{j=0}^{n_x-1} u_j^n e^{-i\frac{2\pi k}{L}(x_j - x_{min})}$ denotes the discrete Fourier transform (DFT) of u_j^0, which can efficiently computed by the fast Fourier transform (FFT).

For the time propagation of the **potential part**

$$i\hbar\partial_t u = V(x)u + \lambda|u|^2 u,$$

because $|u|$ is left invariant it suffices to solve the equation

$$i\hbar\partial_t u = V(x)u + \lambda|u|^2 u$$

which is a linear ODE and again can be exactly integrated in time. The solution is of the form

$$u_j^1 = e^{-i(V(x_j) + \lambda|u_j^0|^2)\triangle t/\hbar} u_j^0.$$

As it is used in the computations of the BEC simulation, we present here the **Strang splitting method**:

One time step $u^n \to u^{n+1}$ with step size $\triangle t = t_{n+1} - t_n$ consists of applying one step $u^n \to u^*$ of the potential part with step size $\frac{\triangle t}{2}$, then one step $u^* \to u^{**}$ of the kinetic part with step size $\triangle t$, and again a step $u^{**} \to u^{n+1}$ of the kinetic part with step size $\frac{\triangle t}{2}$. This gives the following scheme:

$$\begin{aligned} u_j^* &= e^{-i(V(x_j) + \lambda|u_j^n|^2)\triangle t/2\hbar} u_j^n \\ u_j^{**} &= \frac{1}{n_x} \sum_{k=-n_x/2}^{n_x/2-1} e^{-i\hbar\triangle t\ \gamma_k^2/2} \hat{u}_k^* e^{i\gamma_k(x_j - x_{min})} \\ u_j^{n+1} &= e^{-i(V(x_j) + \lambda|u_j^n|^2)\triangle t/2\hbar} u_j^{**} \end{aligned}$$

for $j = 0, \ldots, n_x - 1$ with $\gamma_k = \frac{2\pi k}{x_{max} - x_{min}}$, $\hat{u}_k^n) = \sum_{j=0}^{n_x-1} u_j^* e^{-i\gamma_k(x_j - x_{min})}$.

The advantage of this method is that it is unconditionally stable, it is time reversible as well as time-transverse invariant and satisfies the mass conservation, i.e.: $\|u^n\|_2 = \|u^0\|_2$ for $n = 1, 2, \ldots$.Accuracy is of second order in

time and the spatial discretization is of spectral order of accuracy.

The use of FFT methods requires periodic boundary conditions for the finite computational domain. Physically these conditions clearly don't agree with the behavior of the condensate in the whole space. But choosing a big enough discretization domain that includes the finite support of the trapped condensate, no additional boundary conditions become necessary.

Applying the Strang splitting spectral scheme on the GPE with a **time-dependent potential** $V(x,t)$, the kinetic part remains the same, but the potential part becomes *inhomogeneous* in time:

$$i\hbar\partial_t u(x,t) = V(x,t)u + \lambda|u^n(x,t)|^2 u$$

We approximate the integration of the linear potential term by evaluating it at the center of the respective time intervals which ensures that the accuracy of the scheme remains second order in time. The resulting algorithm is of the form

$$\begin{aligned} u_j^* &= e^{-i(V(t_n+\frac{\triangle t}{4})+\lambda|u_j^n|^2)\triangle t/2\hbar} u_j^n \\ u_j^{**} &= \frac{1}{n_x}\sum_{k=-n_x/2}^{n_x/2-1} e^{-i\hbar\triangle t\ \gamma_k^2/2}\hat{u}_k^* e^{i\gamma_k(x_j-x_{min})} \\ u_j^{n+1} &= e^{-i(V(t_n+\frac{3\triangle t}{4})+\lambda|u_j^n|^2)\triangle t/2\hbar} u_j^{**} \end{aligned}$$

for $j = 0,\ldots,n_x-1$ with $\gamma_k = \frac{2\pi k}{x_{max}-x_{min}}$, $\hat{u}_k^n = \sum_{j=0}^{n_x-1} u_j^n e^{-i\gamma_k(x_j-x_{min})}$.

4.3.2 Free Evolution

The ballistic expansion of the condensate can be modeled by evolving the GPE+ with the confined potential removed. We initialize the solution of the confining regime at $t = T_1$ and continue to solve the GPE for $T_1 \le t \le T_2 = N_2\triangle t$:

$$i\hbar\frac{\partial}{\partial t}u(x,t) = -\frac{\hbar^2}{2m}\triangle u(x,t) + \lambda|u(x,t)|^2 u(x,t)$$

For the computational simulation we can use the same numerical method as in the case above with setting $V \equiv 0$.

In this regime the wave function is not forced to stay in the discretization domain anymore and seeks to expand freely over the whole space. But since we are using again the Strang-Splitting-Spectral scheme, periodic boundary conditions are still required. This induces nonphysical wave interactions which are inappropriate for the behavior of BECs.
Thus one has to improve further appropriate conditions on the artificially generated boundary. Here we chose an absorbing boundary layer method with an additional complex absorbing potential. Therefore we add a boundary layer of width $k\triangle x$ on which we let act an additional complex (pruely imaginary) potential V_C. With this approach, one has to solve the modified GPE

$$i\hbar\frac{\partial}{\partial t}u(x,t) = -\frac{\hbar^2}{2m}\triangle u(x,t) + V_C(y)u(x,t) + \lambda|u(x,t)|^2u(x,t)$$

on $[\tilde{x}_{min}, \tilde{x}_{max}] = [x_{min} - k\triangle x, x_{max} + k\triangle x]$, i.e.: $j = 0, \ldots, n_x + 2k =: \tilde{n}_x$. The absorbing potential $V_C(x)$ satisfies the conditions in Section 4 of Chapter 2. In particular, $V_C(x)$ is defined as zero on the regular domain and has a negative imaginary part on the boundary layer.

Then we apply the same SSS scheme as for the confined scheme on the extended domain $[\tilde{x}_{min}, \tilde{x}_{max}]$ such that

$$\begin{aligned} u_j^* &= e^{-i\lambda|u_j^n|^2\triangle t/2\hbar}u_j^n \\ u_j^{**} &= \frac{1}{n_x}\sum_{k=-\tilde{n}_x/2}^{\tilde{n}_x/2-1} e^{-i\hbar\triangle t\ \gamma_k^2/2}\hat{u}_k^* e^{i\gamma_k(\tilde{x}_j-\tilde{x}_{min})} \\ u_j^{***} &= e^{-i\lambda|u_j^n|^2\triangle t/2\hbar}u_j^{**} \end{aligned}$$

for $j = 0, \ldots, \tilde{n}_x$ with $\gamma_k = \frac{2\pi k}{y_{max}-y_{min}}$, $\hat{u}_k^n = \sum_{j=0}^{n_x-1} u_j^n e^{-i\gamma_k(\tilde{x}_j-\tilde{x}_{min})}$ and append a further step

$$u_j^{n+1} = e^{-V_C(\tilde{x}_j)\triangle t/\hbar}u_j^{***}$$

Here the potential is of a damping nature, which mostly absorbs the outgoing waves, instead of a confining nature.

After some time of spreading, it is physically intuitive to assume that the nonlinear term which comes from the particle interaction becomes negligible. Even tough there is no rigorous derivation for analytical legitimation yet, one can check that resulting differences are insignificant. Thus for the final evolution, i.e.: $t \in [T_2, T]$ we solve the simplified model

$$i\hbar\frac{\partial u(x,t)}{\partial t} = -\frac{\hbar^2}{2m}\triangle u(x,t)$$

This corresponds to the propagation of the kinetic part as described in section 4.3.1. Since this time propagation is exact, we may always use the wave function at $t = T_2$ as initial data u^0 for the calculation of the wave function u^1 at some output time $t \in [T_2, T]$. Due to the rapid spreading of the wave packet, one has to expand the computational domain so that the final wave function u^1 can be represented on this expanded domain; whereas the initial wave function u^0 is zero over a wide range of this domain. To avoid the large amount of memory needed for this expanded domain, we utilize some kind of pruned FFT for the discrete Fourier transforms. Here the augmented zeros of u^0 are not explicitly stored, and only the most significant Fourier coefficients of u^1 are calculated, resulting in a reduced spatial resolution of the output wave function u^1.

Chapter 5

Example: BEC with Rubidium atoms

Finally we present, as an example of atoms with repulsive interaction, a Bose-Einstein condensate of ^{87}Rb atoms according to experiments of the AtomChip group.

5.1 Implementation

The numerical algorithm was implemented in FORTRAN and computed on an Intel Xeon processor with 4GB RAM, however computers with at least 2GB RAM should suffice.
In order to simplify the transfer of the numerical results between computers, the data are stored in the Hierarchical Data Format HDF5 which is a library implementing a multi-object file format. The HDF distribution is freely available from http://www.hdfgroup.org/HDF5/.

For the computation we chose the number of atoms to $N = 10000$, the atomic mass $m = 87 * 1.6605387 \times 10^{-27}$kg, the s-wave length $a = 5.238 \times 10^{-9}$m and the Planck constant $\hbar = 1.05457168 \times 10^{-34}$Js.

Once the ground state is calculated, the simulation is performed in the confining trap regime until $t = 20$ms. After a sudden switch-off of the external potential, the simulation is pursued in the free expansion regime for another 7ms. Therefore the numerical model has to be changed in the spatial and time scale during the computation in order to get satisfactory detailed infor-

mation on the wave function.

Ground state

For the numerical simulation we start with the computation of the of ground state on a three dimensional finite box with ranges

$$\begin{aligned} x: &\quad -4\times10^{-6}\mathrm{m}\ldots 4\times10^{-6}\mathrm{m}\\ y: &\quad -4\times10^{-6}\mathrm{m}\ldots 4\times10^{-6}\mathrm{m}\\ z: &\quad -200\times10^{-6}\mathrm{m}\ldots 200\times10^{-6}\mathrm{m} \end{aligned}$$

which is discretized on a $128\times128\times128$ grid where the spatial step sizes are $\triangle x, \triangle y = \frac{1}{16}\times10^{-6}\mathrm{m} = 0.0625\times10^{-6}\mathrm{m}$, $\triangle z = 3.125\times10^{-6}\mathrm{m}$ and the time step size for ITP is set to $\triangle\tau = 1\times10^{-4}\mathrm{ms}$. The convergence criterion is determined by $\triangle E_0 < 0.5\times10^{-32}\mathrm{J}$. The computation finishes after 144 iterations with $\triangle E_0 = 0.4976\times10^{-32}\mathrm{J}$ while $E_0 = \langle u|H|u\rangle = 0.3156\times10^{-28}\mathrm{J}$ at the end of the iteration.

Time propagation

Stage 1. For $t\in[0,20]\mathrm{ms}$ the simulation proceeds with the time propagation of the GPE on the domain

$$\begin{aligned} x: &\quad -4\times10^{-6}\mathrm{m}\ldots 4\times10^{-6}\mathrm{m}\\ y: &\quad -4\times10^{-6}\mathrm{m}\ldots 4\times10^{-6}\mathrm{m}\\ z: &\quad -200\times10^{-6}\mathrm{m}\ldots 200\times10^{-6}\mathrm{m} \end{aligned}$$

where the time step size is chosen as $\triangle t = 1\times10^{-5}\mathrm{ms}$ with the same spacial scaling as in the ground state computation, i.e. $\triangle x, \triangle y = 0.0625\times10^{-6}\mathrm{m}$, $\triangle z = 3.125\times10^{-6}\mathrm{m}$. This leads to 500 iterations.

Stage 2. For time $t\in[20,21]\mathrm{ms}$, right after the switch-off of the confining trap, the condensate starts to expand which requires an enlargement of the computation domain. In particular, the z-scaling remains unchanged and only the transversal scales are extended to:

$$\begin{aligned} x: &\quad -16\times10^{-6}\mathrm{m}\ldots 16\times10^{-6}\mathrm{m}\\ y: &\quad -16\times10^{-6}\mathrm{m}\ldots 16\times10^{-6}\mathrm{m}\\ z: &\quad -200\times10^{-6}\mathrm{m}\ldots 200\times10^{-6}\mathrm{m}. \end{aligned}$$

This is discretized on a $512\times512\times128$ grid such that the spatial step sizes are still $\triangle x, \triangle y = 0.0625\times10^{-6}\mathrm{m}$, $\triangle z = 3.125\times10^{-6}\mathrm{m}$. Likewise the time

step size is again $\triangle t = 1 \times 10^{-5}$ms in order to obtain a detailed simulation of this section. This gives 100 iterations to guarantee a full representation of the evolution.

Stage 3a. For $t \in [21, 23]$ms, the wave function continues to expand in the transversal direction. Therefore we again enlarge the simulation domain to

$$\begin{aligned} x: &\quad -32 \times 10^{-6}\text{m} \ldots 32 \times 10^{-6}\text{m} \\ y: &\quad -32 \times 10^{-6}\text{m} \ldots 32 \times 10^{-6}\text{m} \\ z: &\quad -200 \times 10^{-6}\text{m} \ldots 200 \times 10^{-6}\text{m}. \end{aligned}$$

Thus the domain would be extended to a $1024 \times 1024 \times 128$ grid. But since in this section the time propagation of the the free Schrödinger equation is implemented using an pruned FFT-method, a $512 \times 512 \times 128$ grid becomes sufficient for the computation. The spatial step sizes are now $\triangle x, \triangle y = \frac{1}{8}10^{-6}\text{m}$ $= 0.125 \times 10^{-6}\text{m}$, $\triangle z = 3.125 \times 10^{-6}\text{m}$. For the time step size we choose $\triangle t = 5 \times 10^{-5}$ms which leads to 40 iterations in this section.

Stage 3b. At the final $t \in [23, 27]$ms, the expansion is proceeded to

$$\begin{aligned} x: &\quad -64 \times 10^{-6}\text{m} \ldots 64 \times 10^{-6}\text{m} \\ y: &\quad -64 \times 10^{-6}\text{m} \ldots 64 \times 10^{-6}\text{m} \\ z: &\quad -200 \times 10^{-6}\text{m} \ldots 200 \times 10^{-6}\text{m}, \end{aligned}$$

which would correspond to a $2048 \times 2048 \times 128$ grid, but again it can be reduced to a $512 \times 512 \times 128$ grid and the spatial step sizes are $\triangle x, \triangle y = \frac{1}{4}10^{-6}\text{m} = 0.25 \times 10^{-6}\text{m}$, $\triangle z = 3.125 \times 10^{-6}\text{m}$. Conclusively, the time step size is again $\triangle t = 5 \times 10^{-5}$ms ms such that the procedure ends after 80 iterations.

5.2 Visualization

The achievement of visualizing simulation data respectively physical phenomena induces a collaboration of mathematical theorists, numeric scientists and research physicists. In order to get a maximum profit of the numerical computations, visualization should be a inherent part in the simulation process. It can provide a solid understanding of physical phenomena or numerical data.

Furthermore, scientific discovery can often be accelerated through computations and visualizations.

Our visualizations are realized with the numerical computing environment MATLAB. We show the probability density of the wave function integrated over the x-, y- and respectively z-axes. For illustration we used a filled contour plot where the density values are assigned to colors according to the specific color map.

The confining regime for $t \in [0, 20]$ms is documented by 9 extracts intensified at the moment of splitting $t \in [9, 12]$ms. The elongated density cloud gets split along the x-axis. The splitting evolution can be observed along the y- and z-axes while it doesn't change its shape essentially seen along the x-axis. Here the observation area can be chosen small according to the trapping region.

The next stage is a focus on the process during the first millisecond right after the trap switch-off, i.e. $t \in [20, 21]$ms. This sequence is documented within 6 figures. One sees that the cloud starts to spread and the density decreases very fast within two orders of magnitude. At the same time interference patterns appear with fringes in the $y \times z$-plane. Due to the spreading the simulation area is expanded by the factor of two in order to observe the propagation properly during the first second after the trap switch-off.

The last section shows further free expansion for $t \in [21, 27]$ms in 7 final samples. The domain is again extended by a factor of 4 such that one can sufficiently follow the expanding propagation. Within this period of time usually physicists generate some pictures with the absorbing imaging method. These pictures are well reconstructed by the numerical simulation as we can see. Nevertheless by the use of numerical visualization not only the resolution can be increased to get beautiful homogenous pictures, in fact it makes it possible to follow the whole propagation process.

In addition, the complete series of data was collected to an animated sequence. We recorded the animations as AVI-formated and MPEG-formated movies.

5.2.1 Time propagation for $t \in [0, 20]$ms

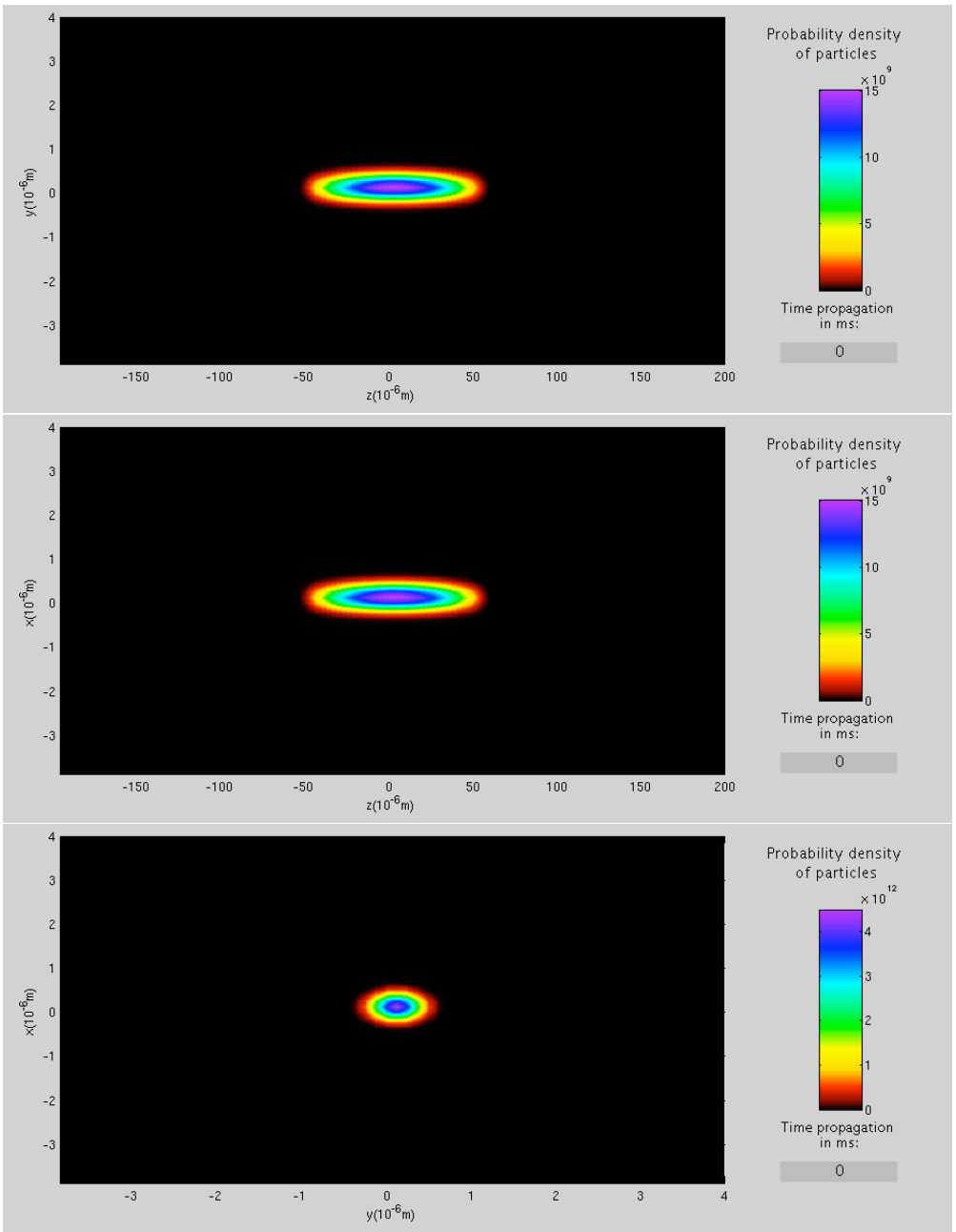

Figure 5.1: Simulation of confined dynamics at $t = 0ms$, integrated over the (a) x-axis, (b) y-axis and (c) z-axis

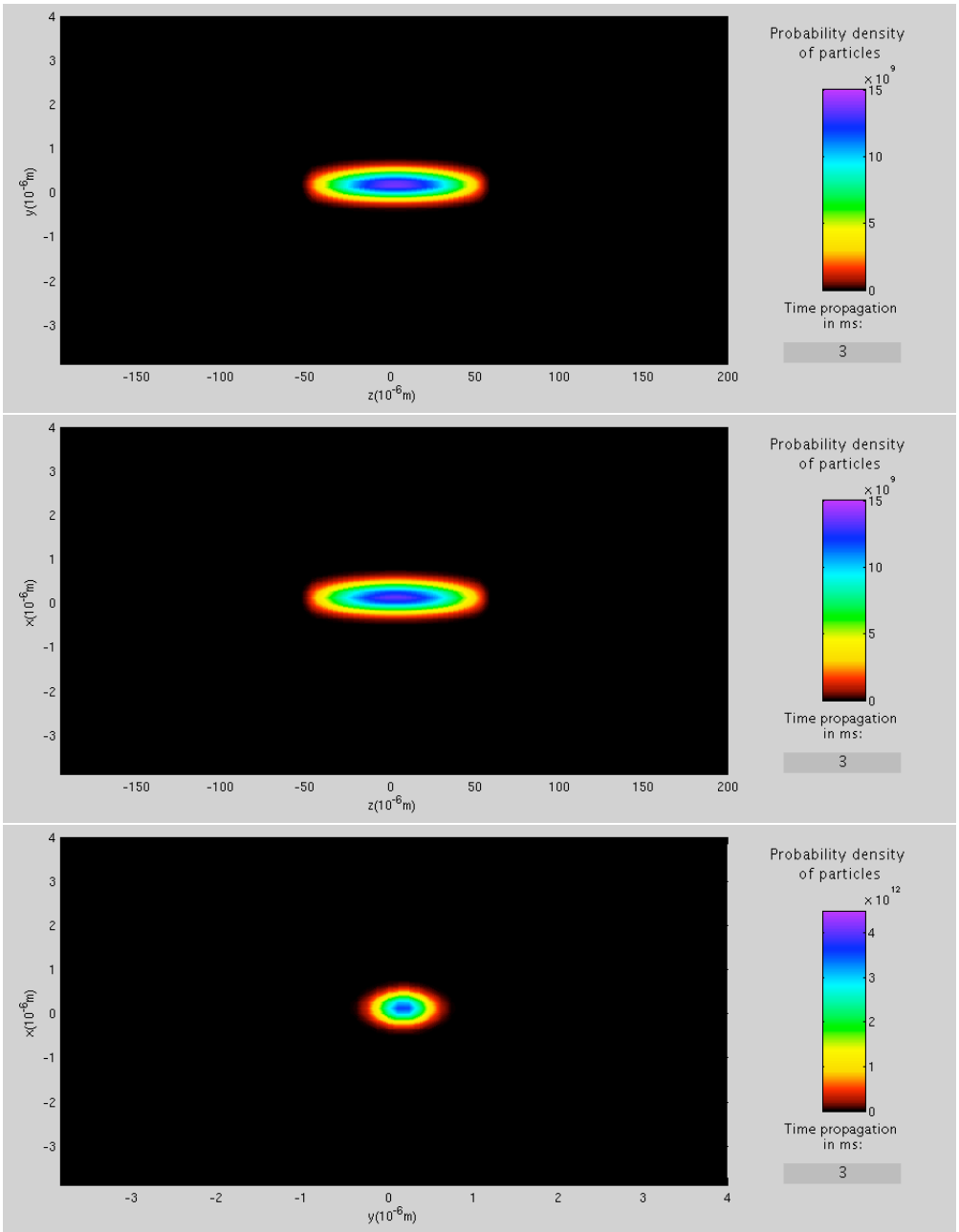

Figure 5.2: Simulation of confined dynamics at $t = 3ms$, integrated over the (a) x-axis, (b) y-axis and (c) z-axis

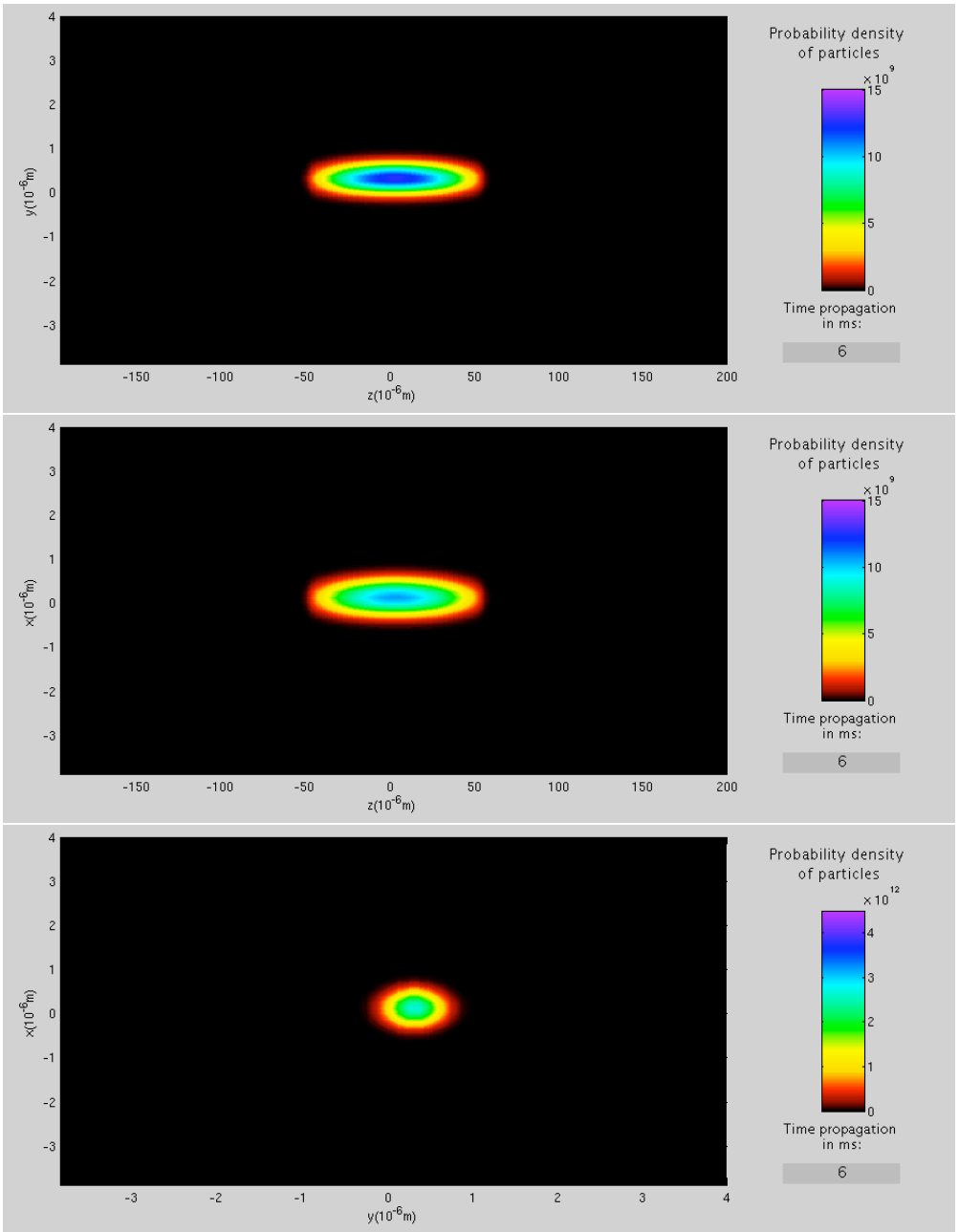

Figure 5.3: Simulation of confined dynamics at $t = 6ms$, integrated over the (a) x-axis, (b) y-axis and (c) z-axis

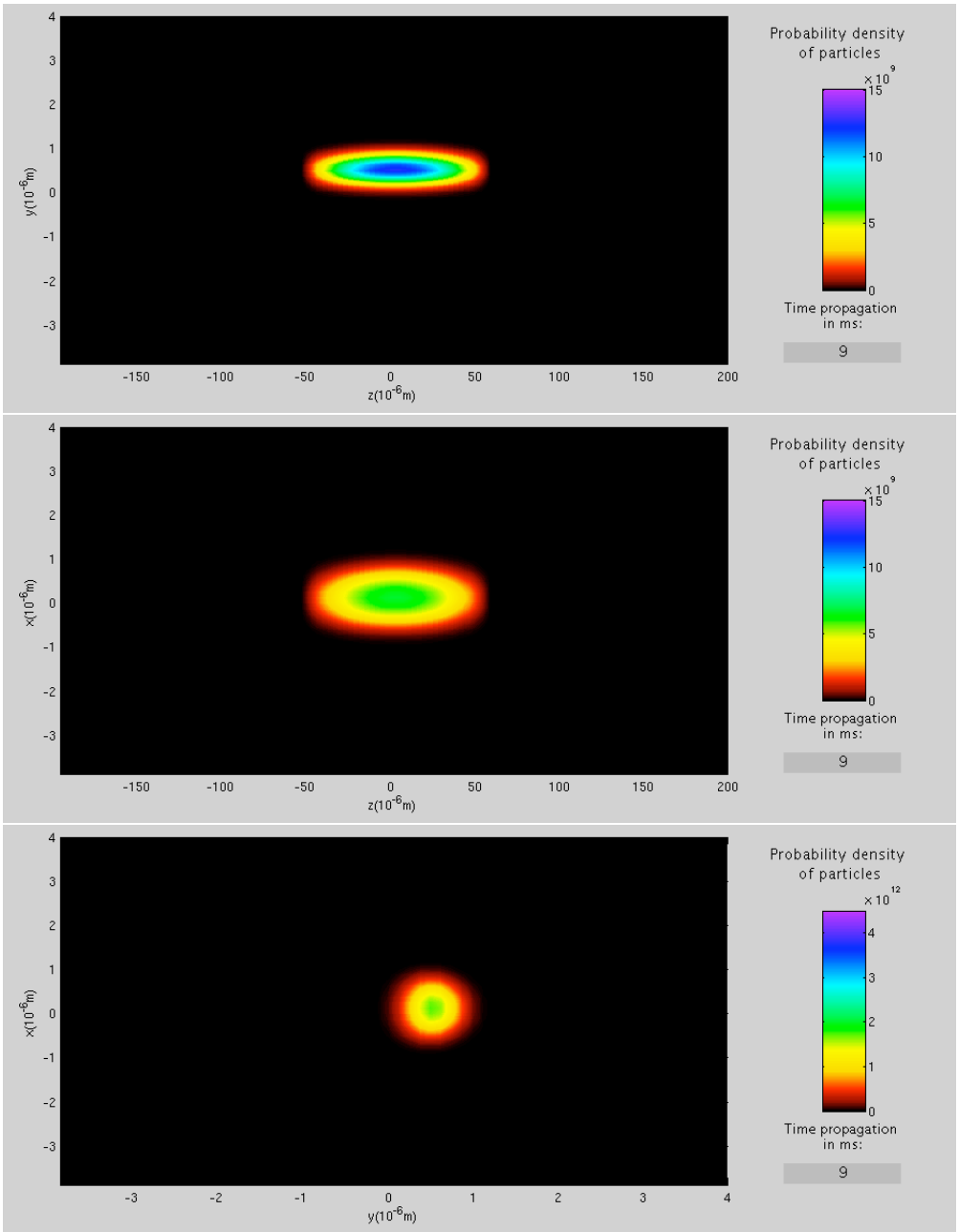

Figure 5.4: Simulation of confined dynamics at $t = 9ms$, integrated over the (a) x-axis, (b) y-axis and (c) z-axis

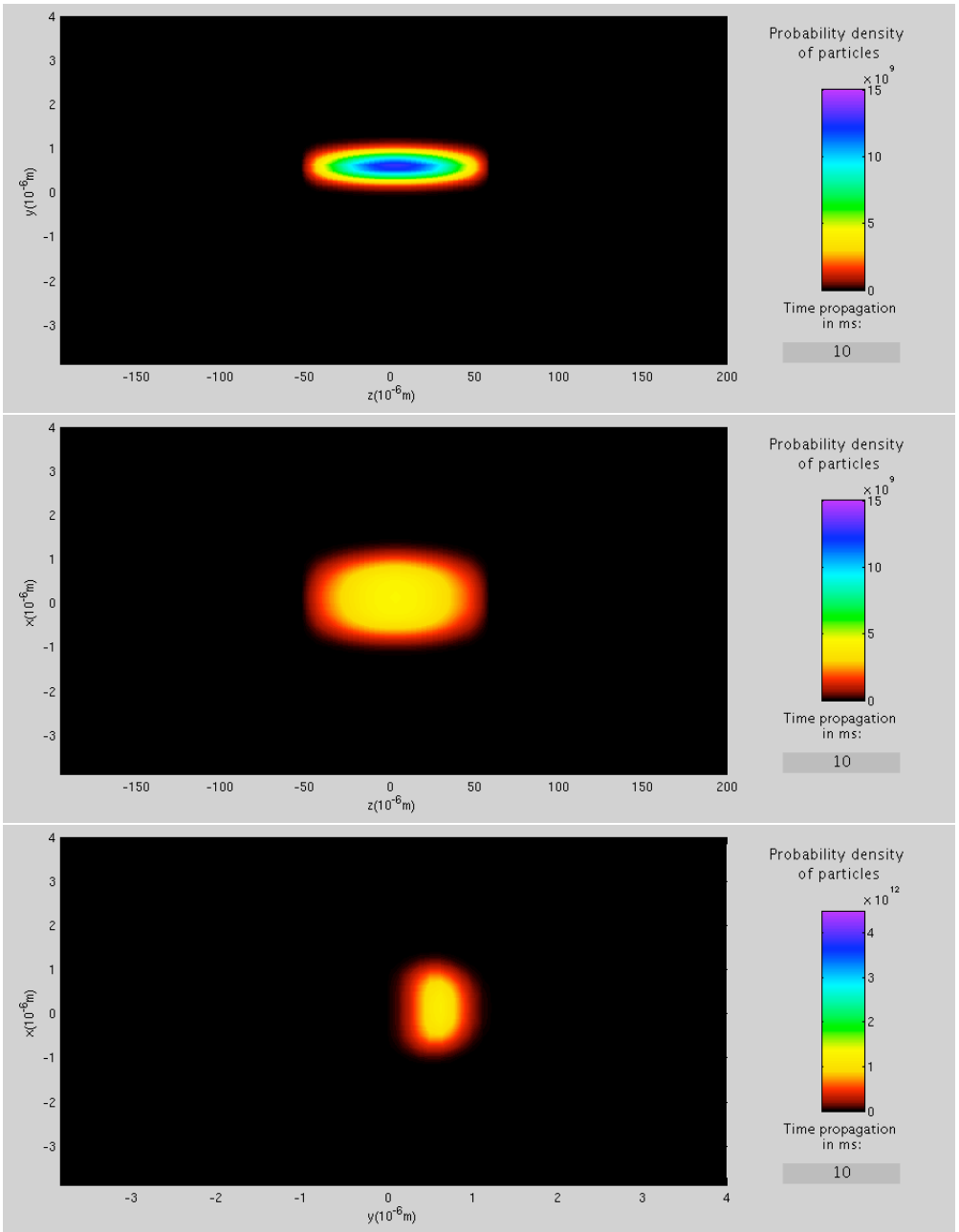

Figure 5.5: Simulation of confined dynamics at $t = 10ms$, integrated over the (a) x-axis, (b) y-axis and (c) z-axis

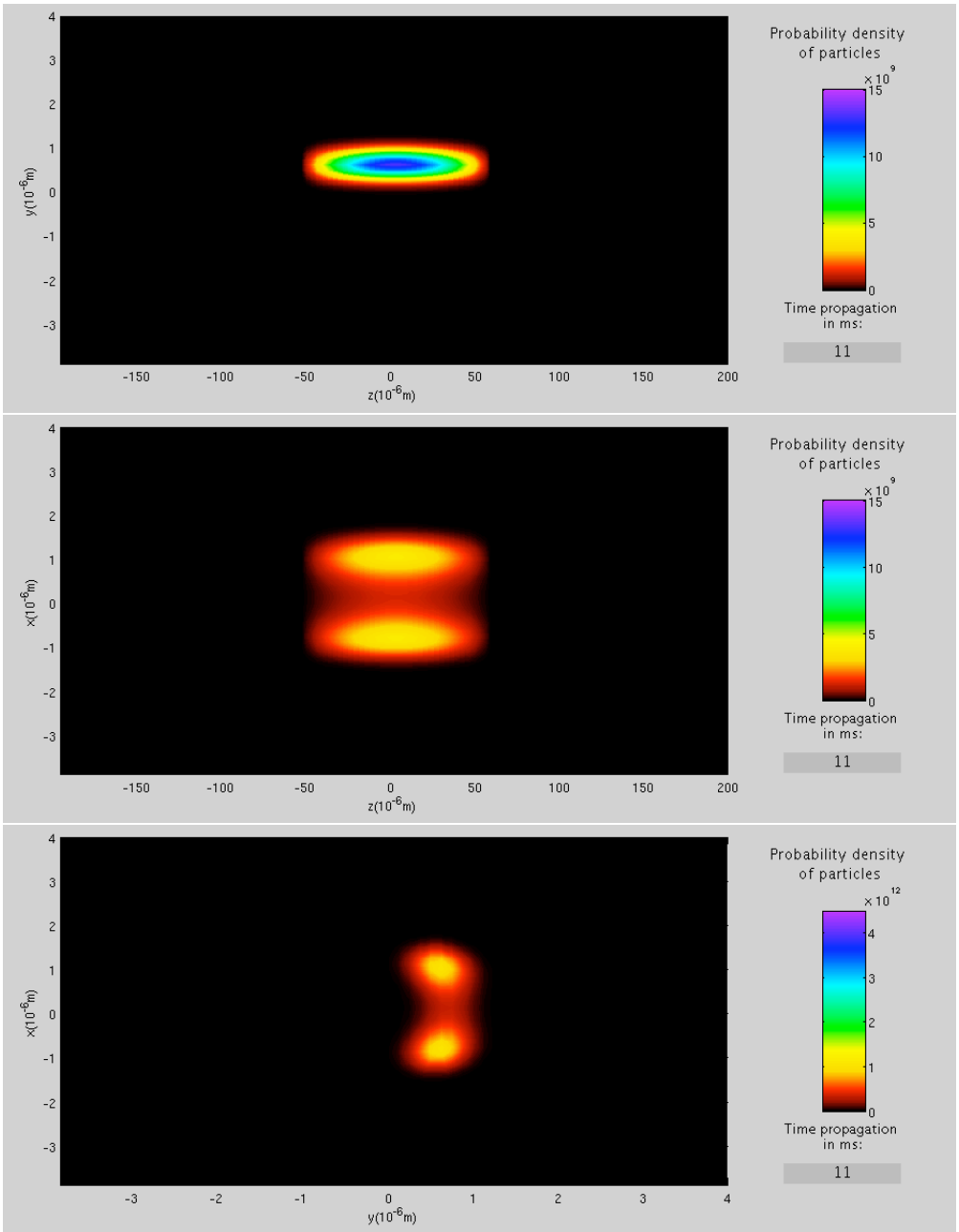

Figure 5.6: Simulation of confined dynamics at $t = 11ms$, integrated over the (a) x-axis, (b) y-axis and (c) z-axis

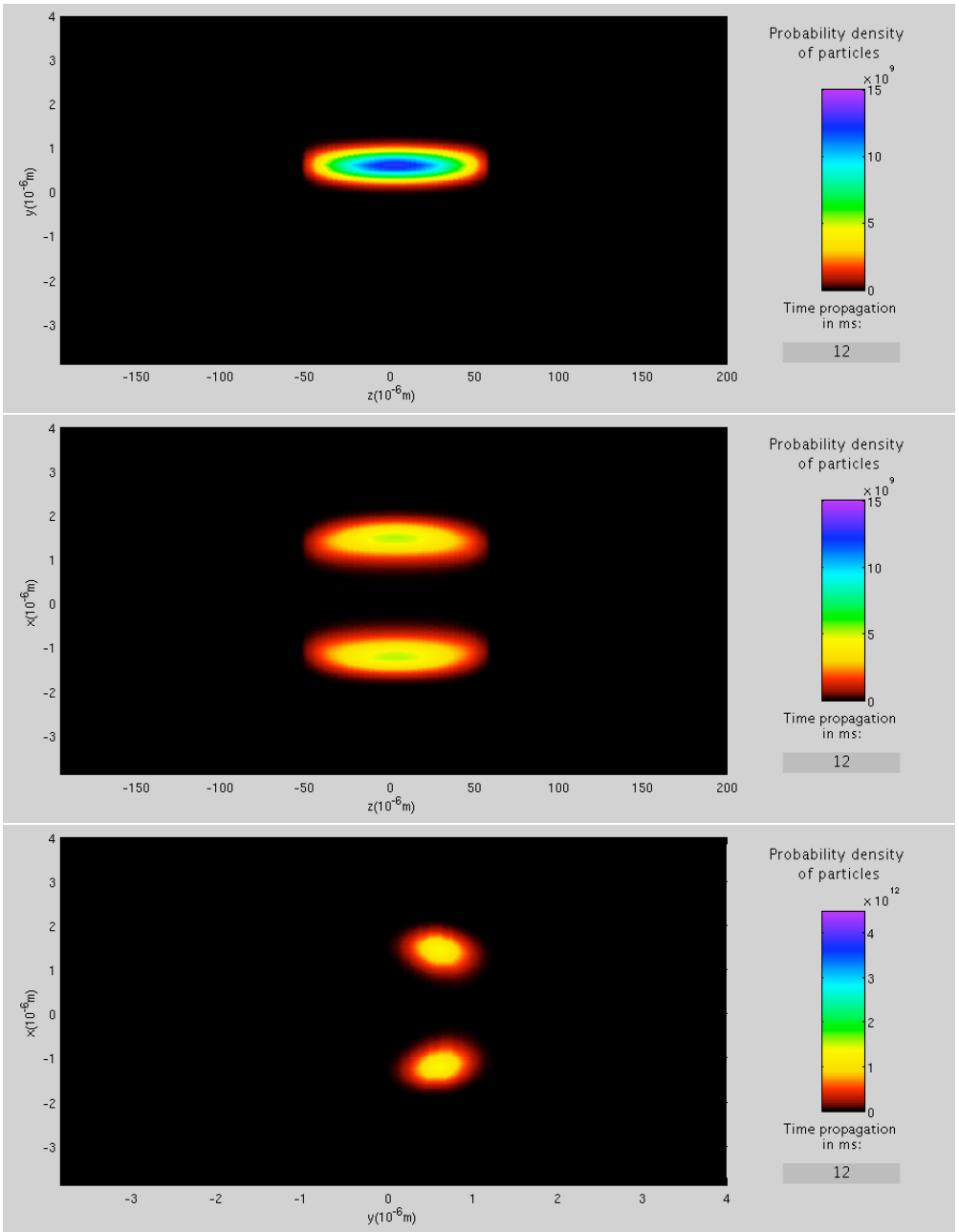

Figure 5.7: Simulation of confined dynamics at $t = 12ms$, integrated over the (a) x-axis, (b) y-axis and (c) z-axis

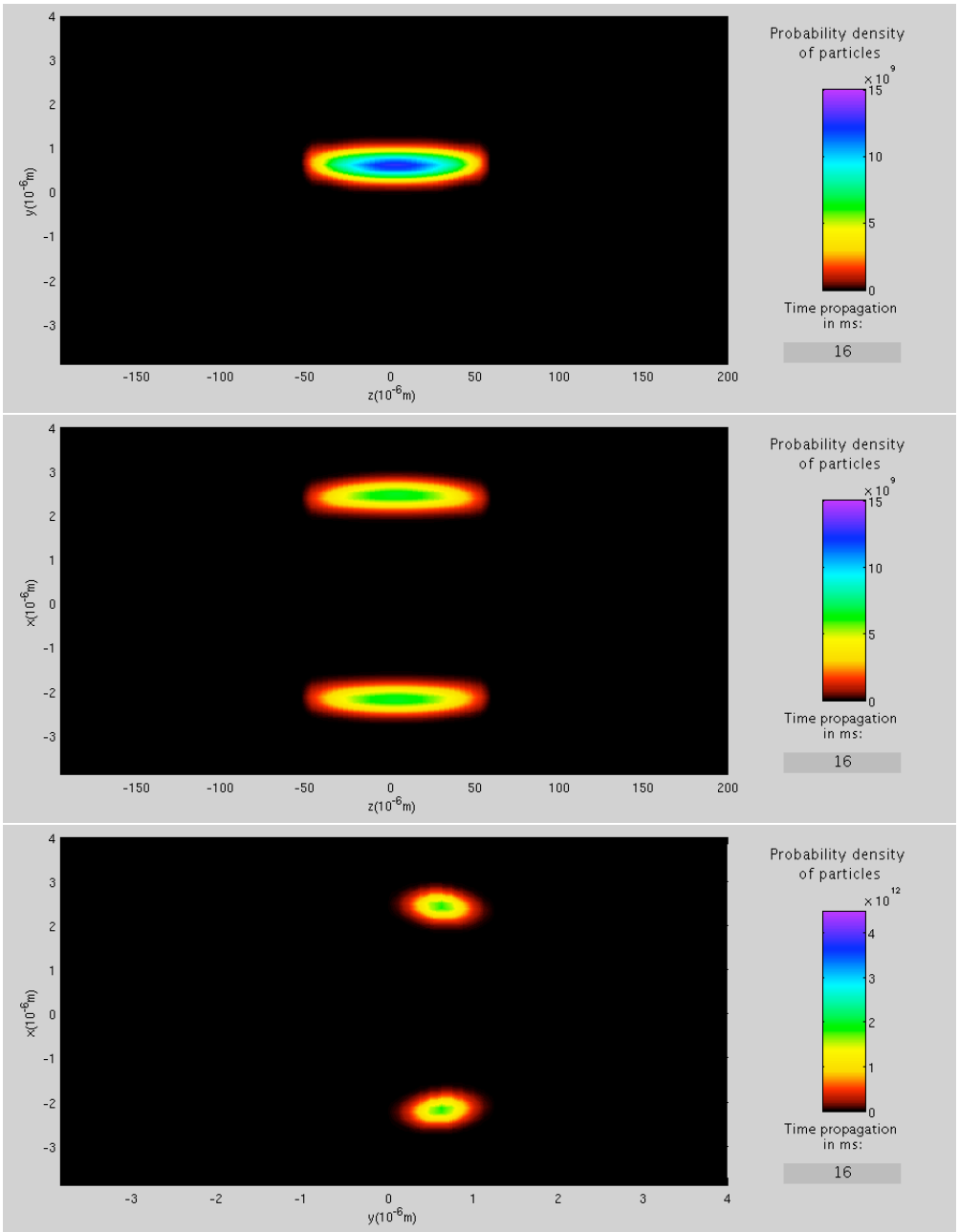

Figure 5.8: Simulation of confined dynamics at $t = 16ms$, integrated over the (a) x-axis, (b) y-axis and (c) z-axis

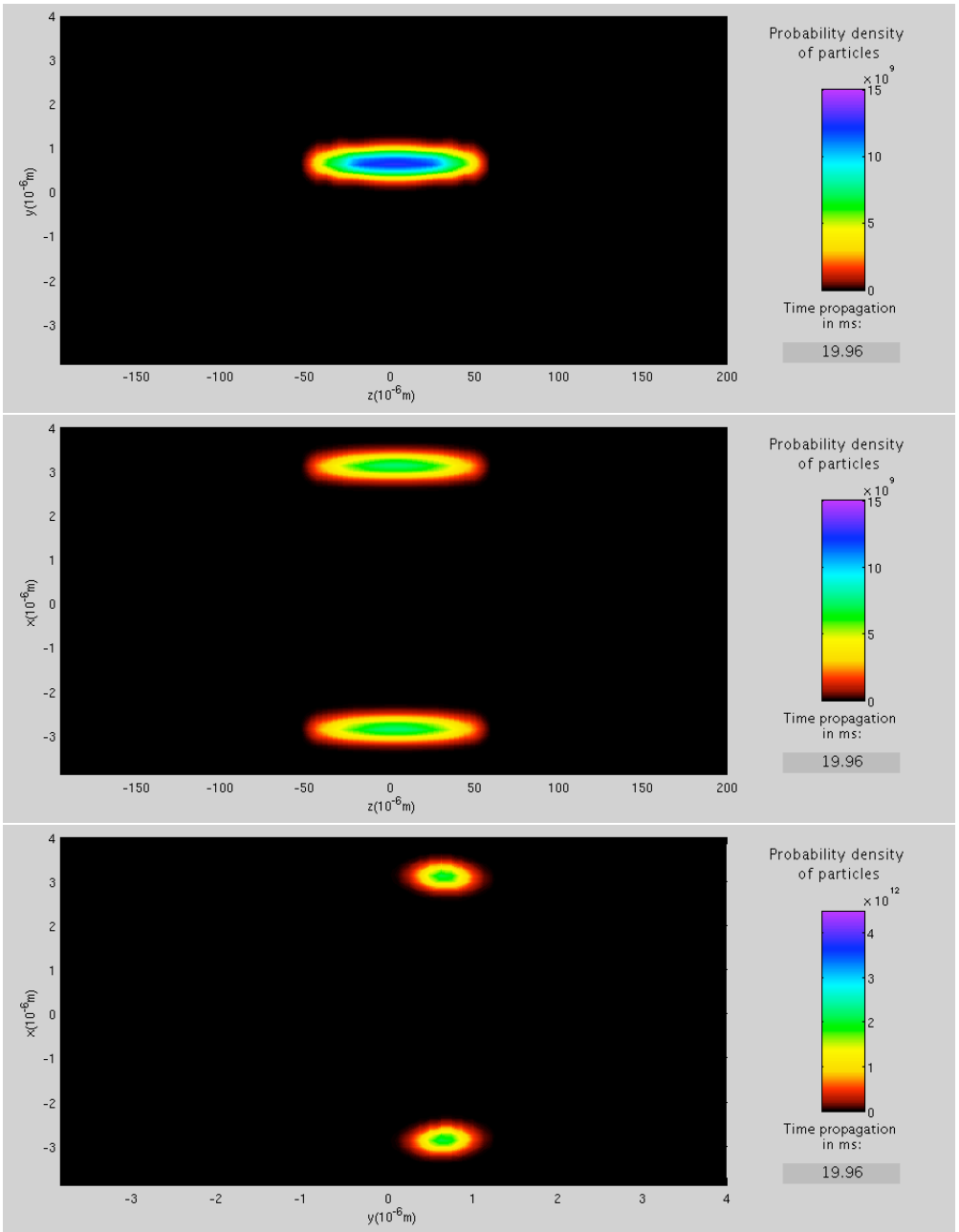

Figure 5.9: Simulation of confined dynamics at $t = 20ms$, integrated over the (a) x-axis, (b) y-axis and (c) z-axis

5.2.2 Time propagation for $t \in [20, 21]$ms

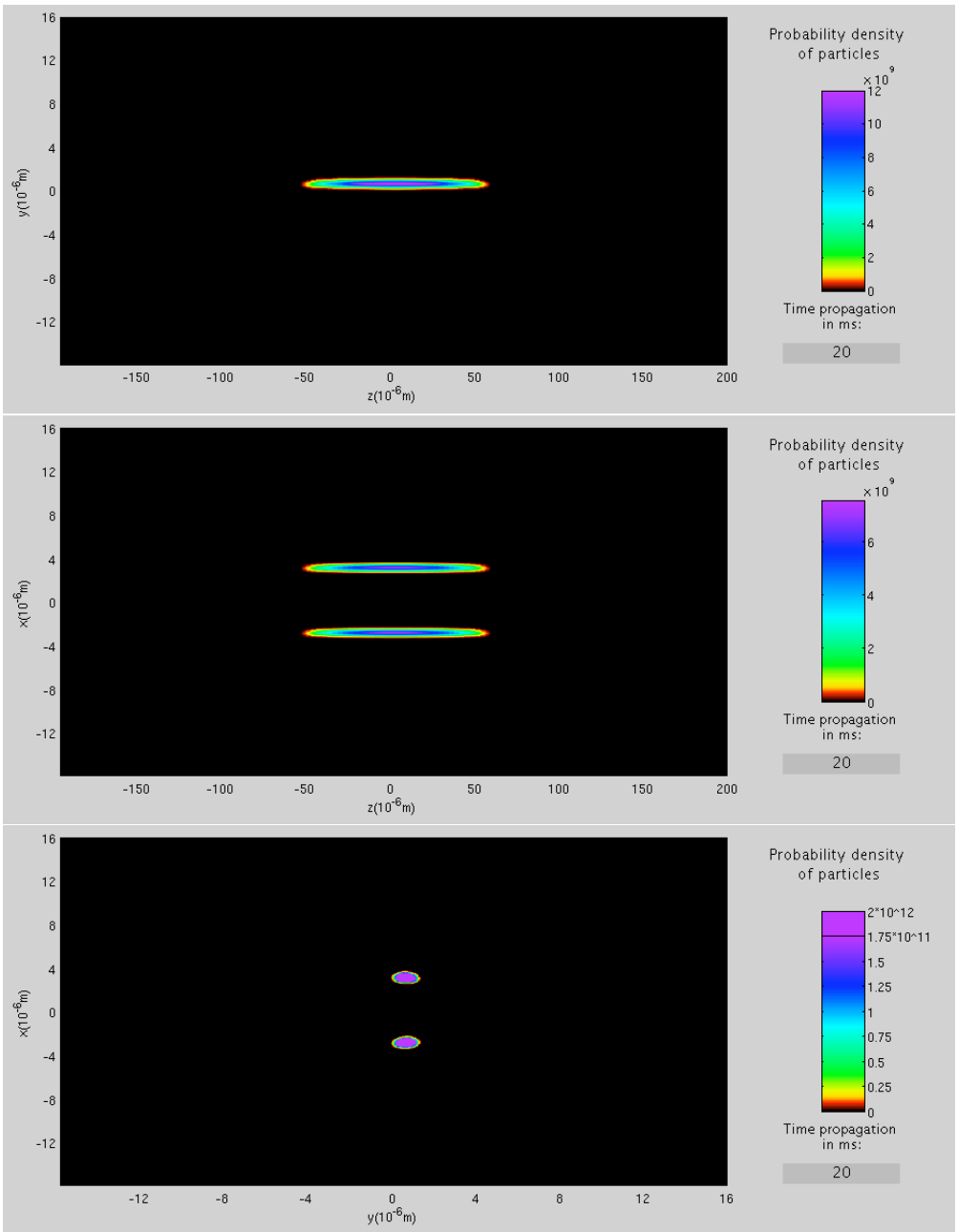

Figure 5.10: Simulation of free expansion at $t = 20ms$, integrated over the (a) x-axis, (b) y-axis and (c) z-axis

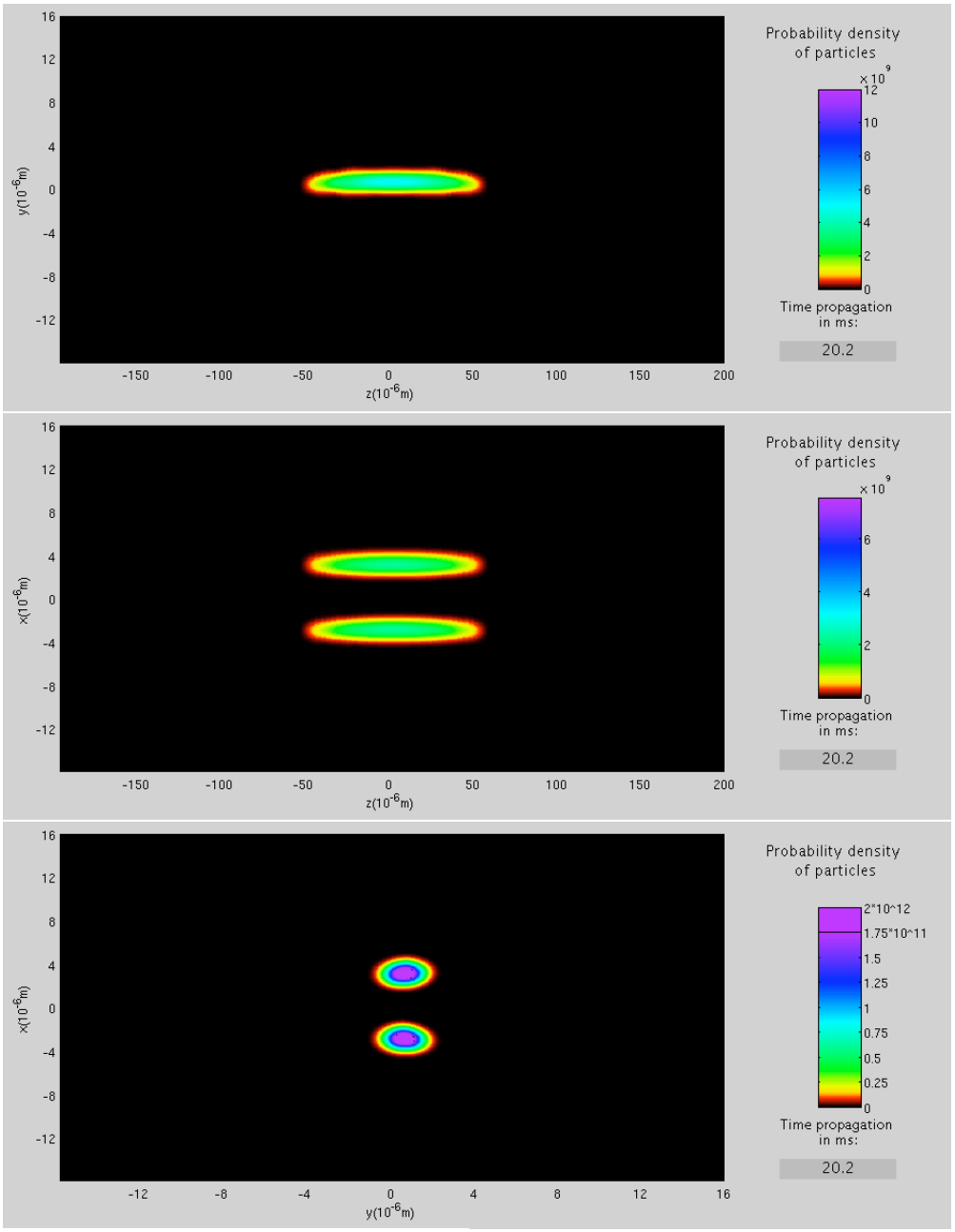

Figure 5.11: Simulation of free expansion at $t = 20.2ms$, integrated over the (a) x-axis, (b) y-axis and (c) z-axis

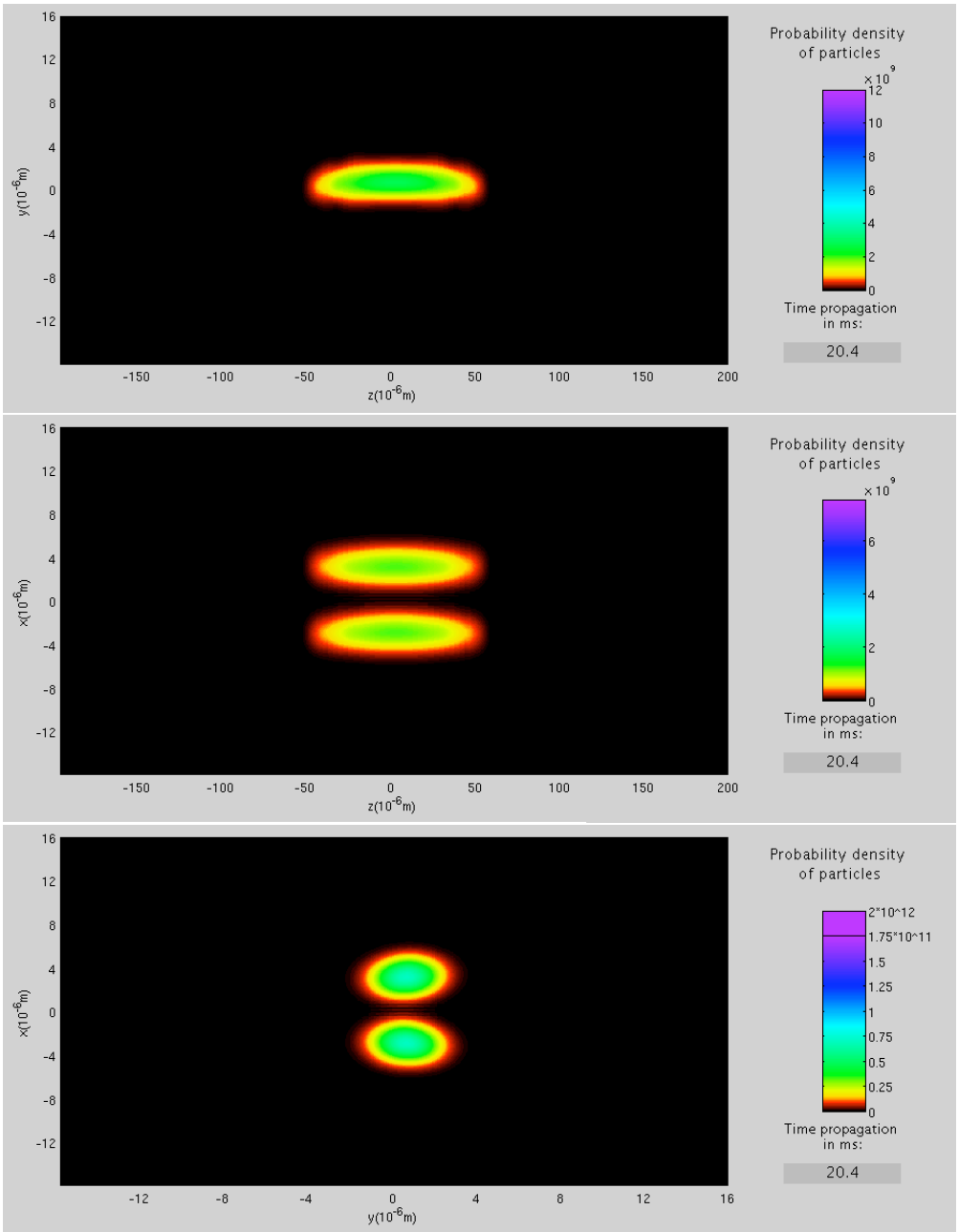

Figure 5.12: Simulation of free expansion at $t = 20.4ms$, integrated over the (a) x-axis, (b) y-axis and (c) z-axis

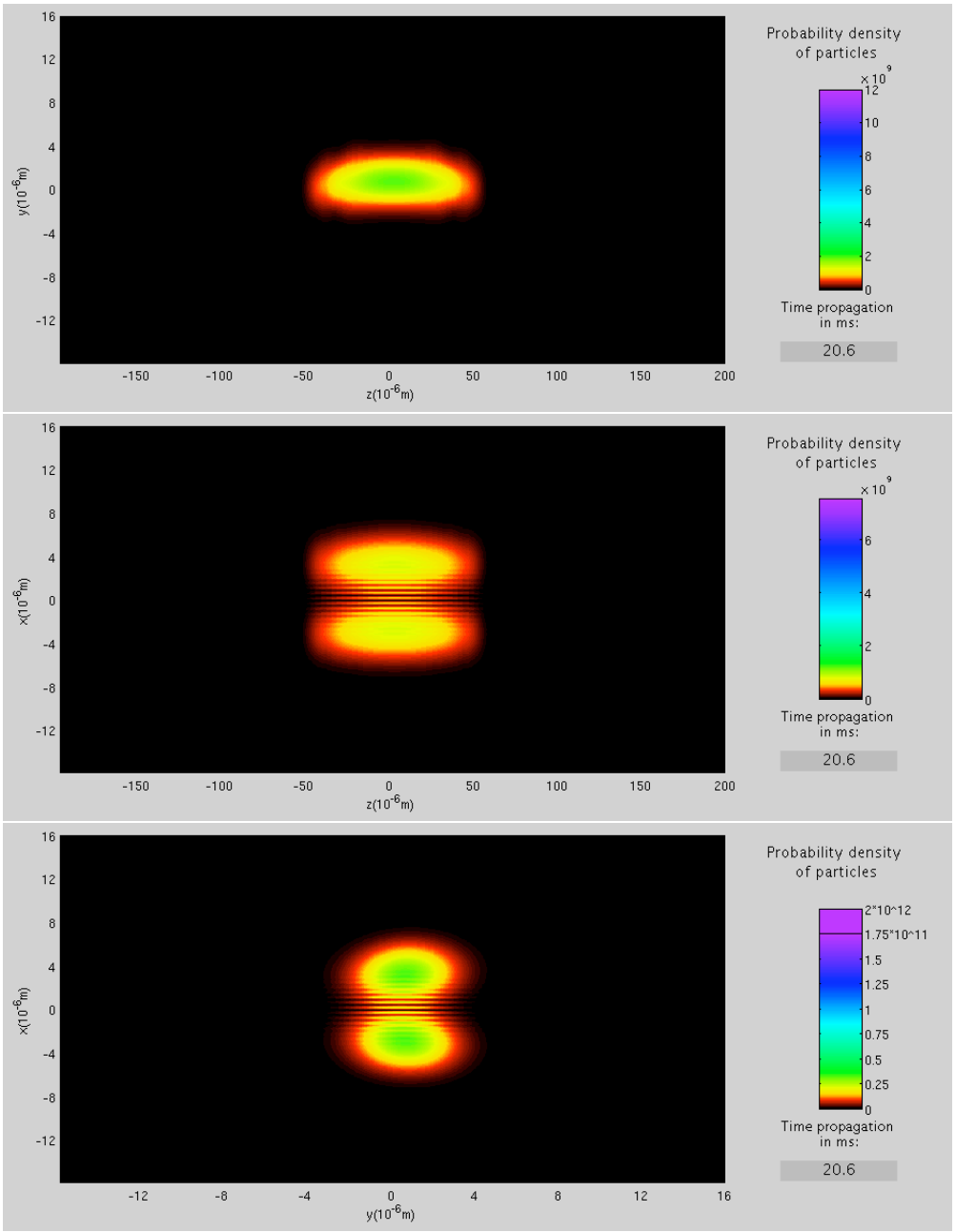

Figure 5.13: Simulation of free expansion at $t = 20.6ms$, integrated over the (a) x-axis, (b) y-axis and (c) z-axis

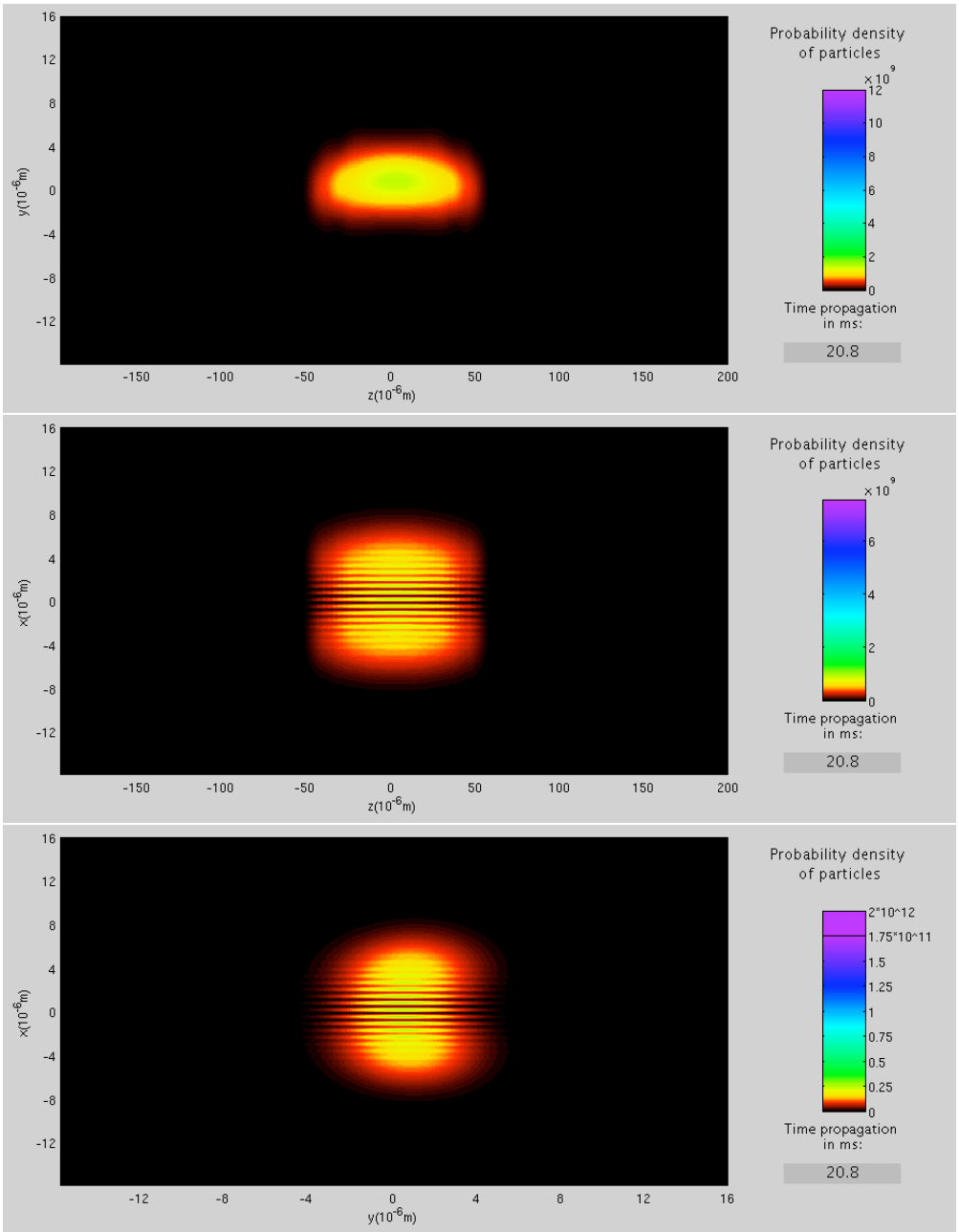

Figure 5.14: Simulation of free expansion at $t = 20.8ms$, integrated over the (a) x-axis, (b) y-axis and (c) z-axis

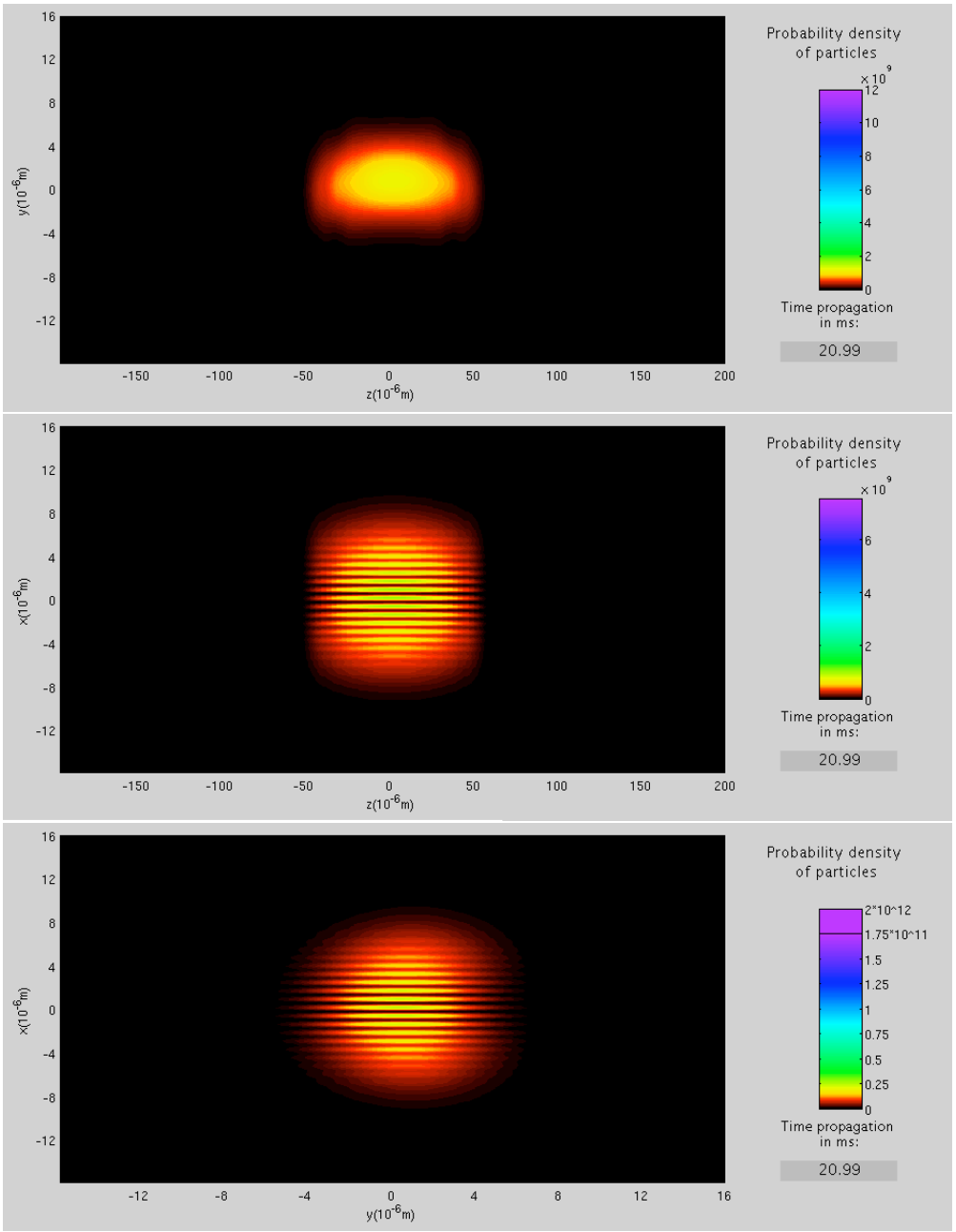

Figure 5.15: Simulation of free expansion at $t = 21ms$, integrated over the (a) x-axis, (b) y-axis and (c) z-axis

5.2.3 Time propagation for $t \in [21, 27]$ms

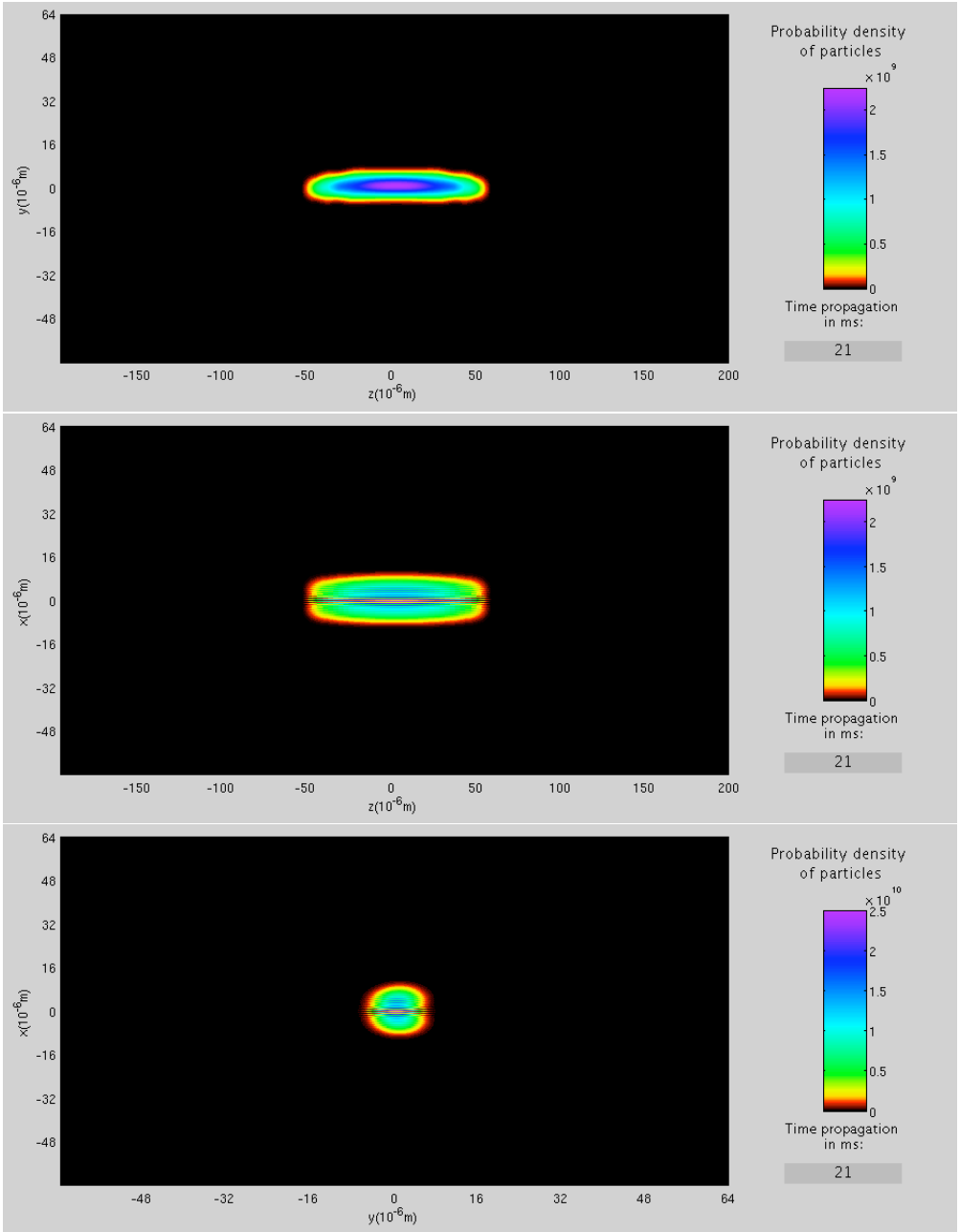

Figure 5.16: Simulation of free expansion at $t = 21ms$, integrated over the (a) x-axis, (b) y-axis and (c) z-axis

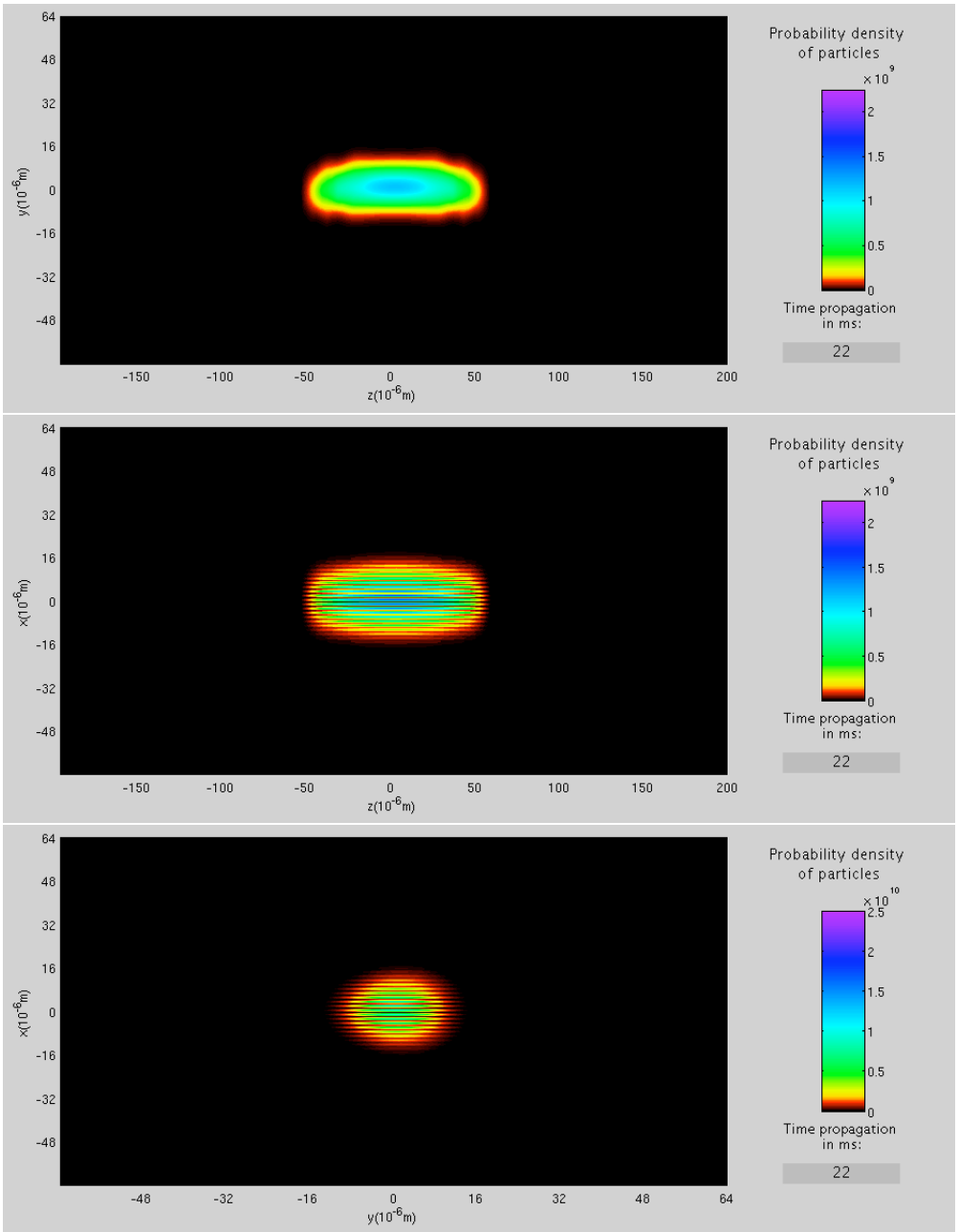

Figure 5.17: Simulation of free expansion at $t = 22ms$, integrated over the (a) x-axis, (b) y-axis and (c) z-axis

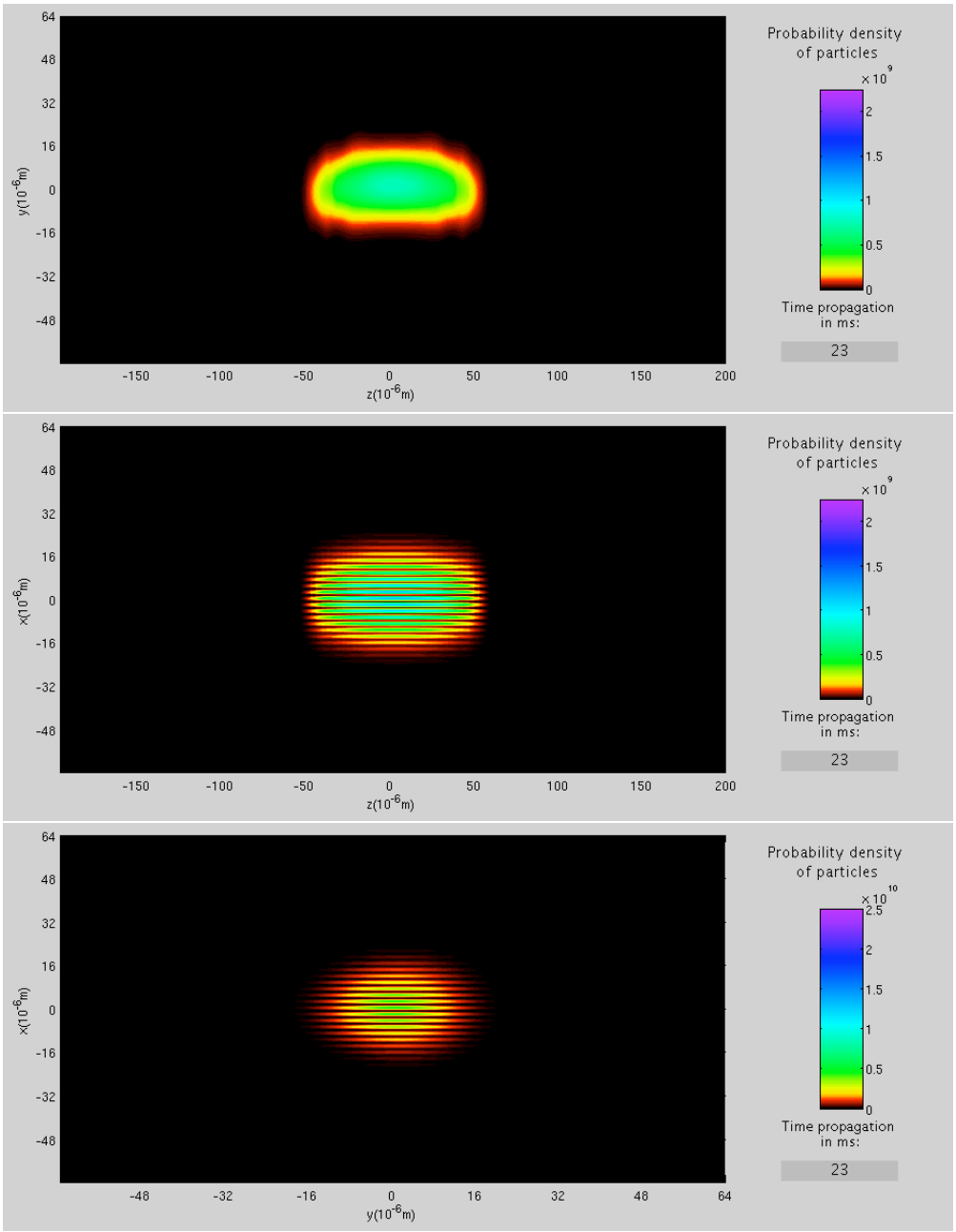

Figure 5.18: Simulation of free expansion at $t = 23ms$, integrated over the (a) x-axis, (b) y-axis and (c) z-axis

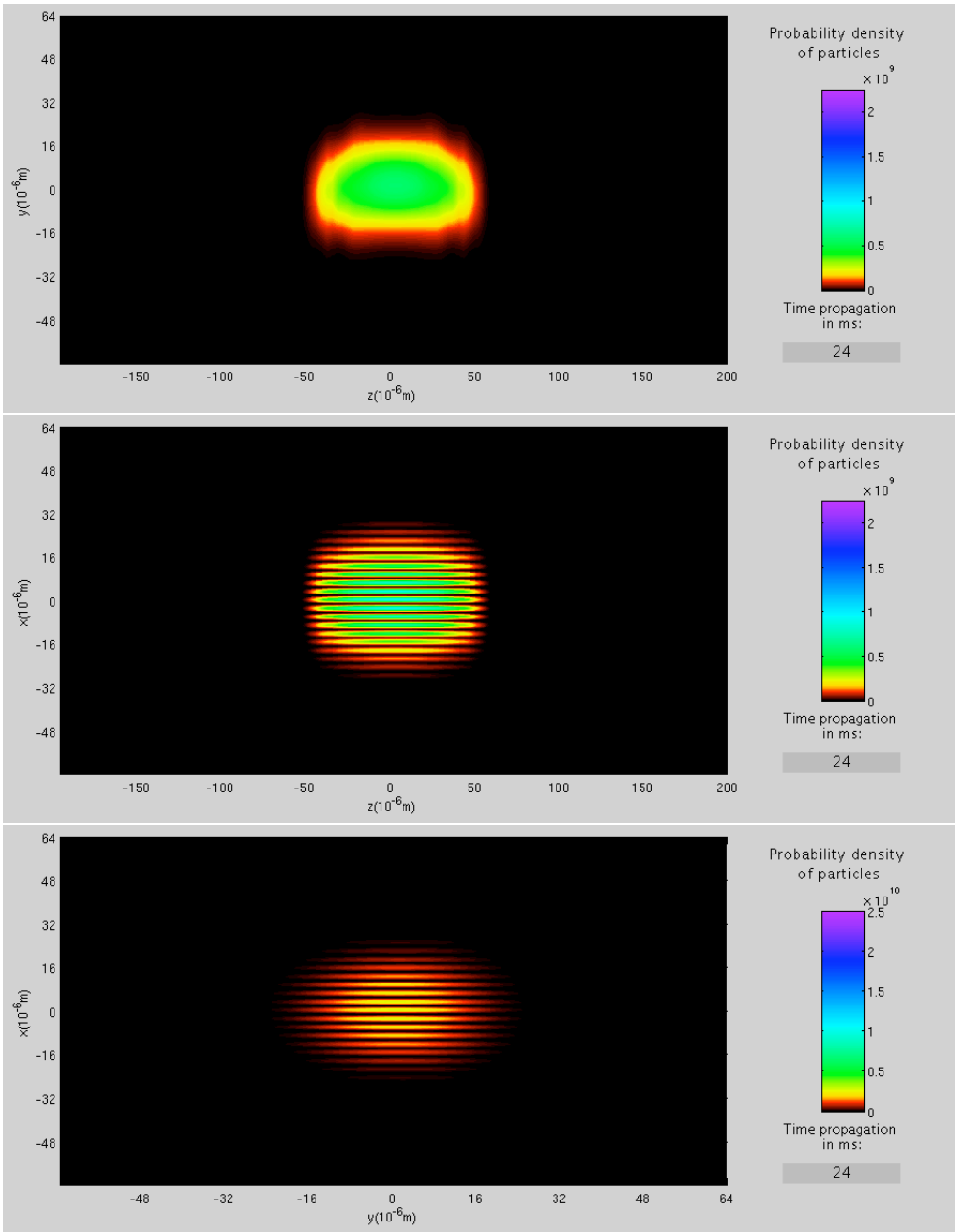

Figure 5.19: Simulation of free expansion at $t = 24ms$, integrated over the (a) x-axis, (b) y-axis and (c) z-axis

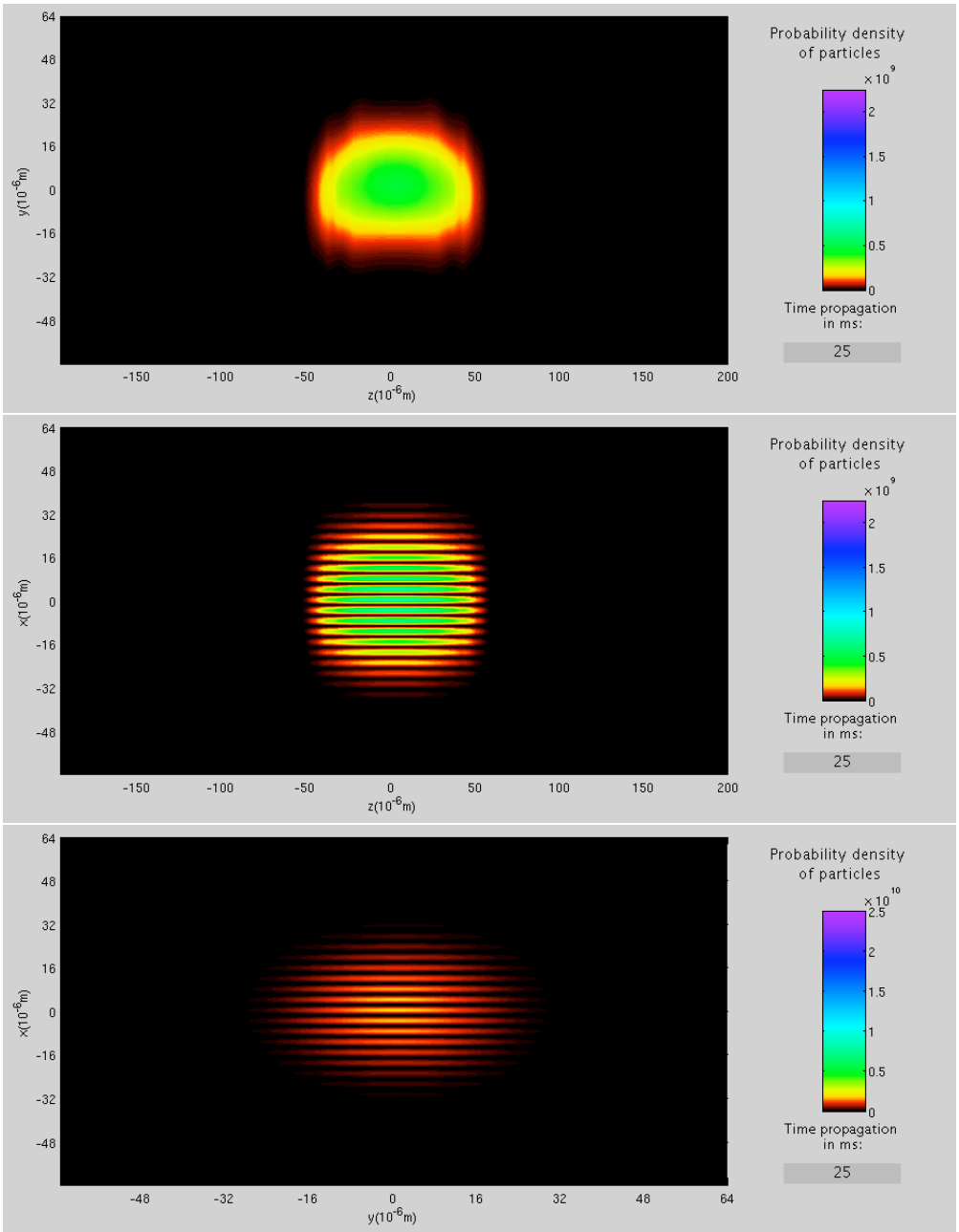

Figure 5.20: Simulation of free expansion at $t = 25ms$, integrated over the (a) x-axis, (b) y-axis and (c) z-axis

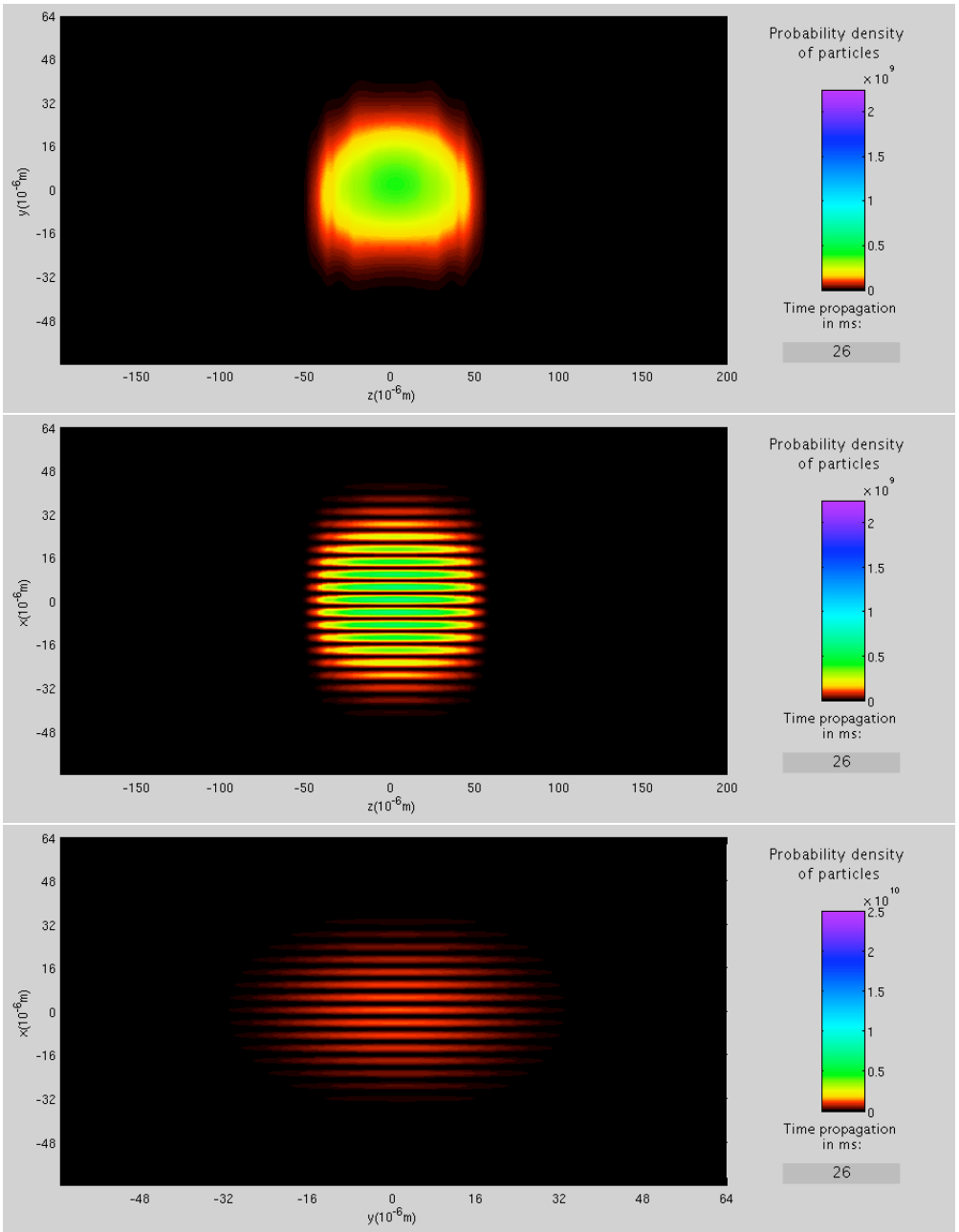

Figure 5.21: Simulation of free expansion at $t = 26ms$, integrated over the (a) x-axis, (b) y-axis and (c) z-axis

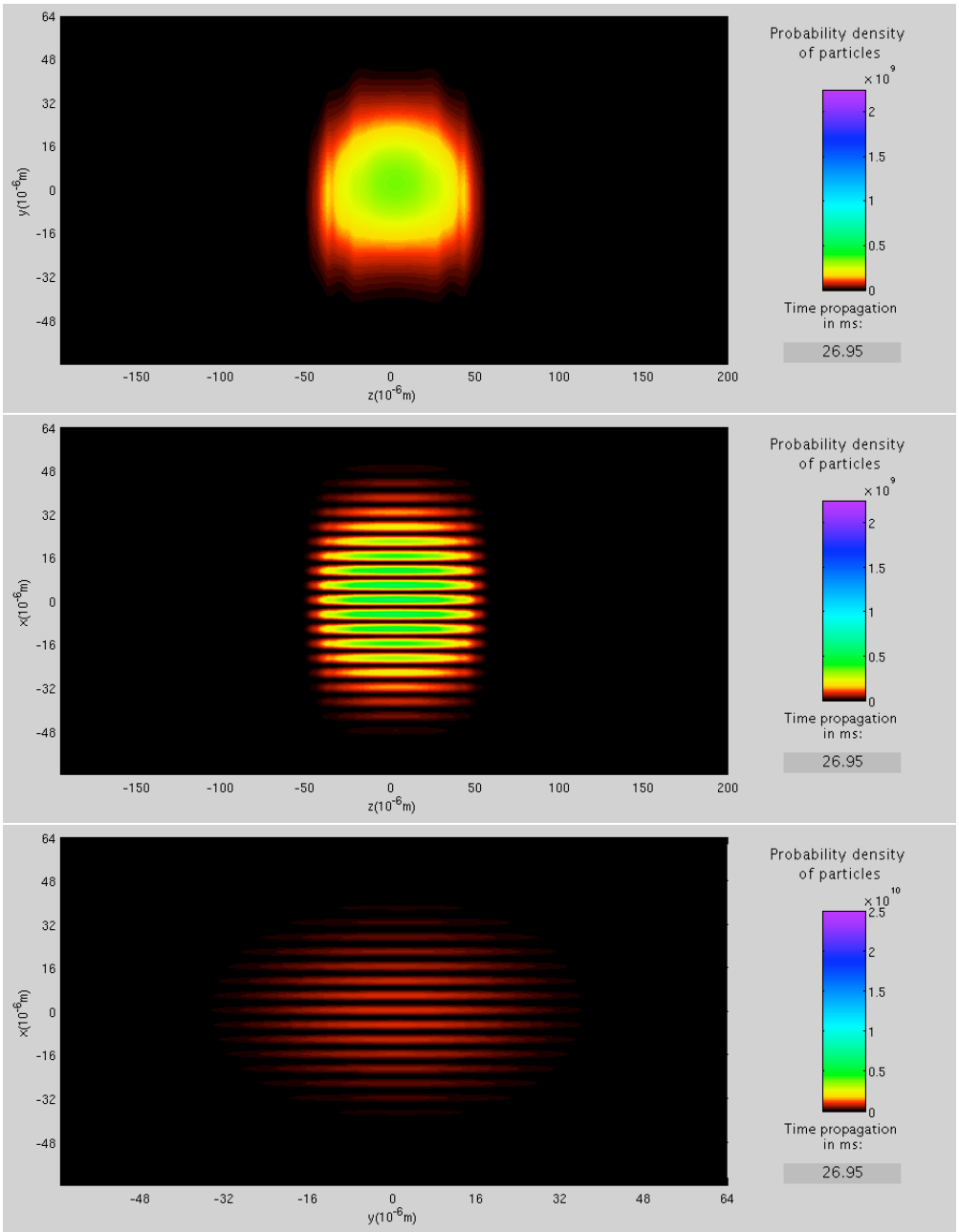

Figure 5.22: Simulation of free expansion at $t = 27ms$, integrated over the (a) x-axis, (b) y-axis and (c) z-axis

Bibliography

[1] N. B. Abdallah, F. Méhats, C. Schmeiser, and R. M. Weishäupl. The Nonlinear Schrödinger Equation with a Strongly Anisotropic Harmonic Potential. *SIAM, J. Math. Analysis*, 37:189, 2005.

[2] S. K. Adhikari. Numerical study of the spherically symmetric Gross-Pitaevskii equation in two space dimensions. *Phys. Review E*, 62:2937, 2000.

[3] S. K. Adhikari and P. Muruganandam. Bose-Einstein condensation dynamics in three dimensions by the pseudospectral and finite-difference methods. *J. Phys. B: At., Mol. and Opt. Phys.*, 36:2501, 2003.

[4] M. H. Anderson, J. R. Ensher, M. R. Matthews, C. E. Wieman, and E. A. Cornell. Observation of Bose-Einstein Condensation in a Dilute Atomic Vapor. *Science*, 269:198, 1995.

[5] R. Anton. Global existence for defocusing cubic NLS and Gross-Pitaevskii equation in three dimensional exterior domains. *arXiv:math/0701304v1*, 2007.

[6] W. Bao and Q. Du. Computing the Ground-state solution of Bose-Einstein condensate by a normalized gradient flow. *SIAM, J. Sci. Computing*, 25:1674, 2004.

[7] W. Bao, D. Jaksch, and P. A. Markowich. Numerical solution of the Gross-Pitaevskii equation for the Bose-Einstein condensation. *J. Comp. Physics*, 187:318, 2003.

[8] W. Bao, S. Jin, and P. A. Markowich. On Time-Splitting Spectral Approximations for the Schrödinger Equation in the Semiclassical Regime. *J. Comp. Physics*, 175:487, 2002.

[9] W. Bao, F. Y. Lim, and Y. Zhang. Energy and Chemical potential asymptotics for the ground state of Bose-Einstein Condensates in the

semi-classical regime. *Bulletin of the Institute of Mathematics*, 2:495, 2007.

[10] W. Bao and W. Tang. Ground-state solution of Bose-Einstein condensate by directly minimizing the energy functional. *J. Comp. Physics*, 187:230, 2003.

[11] R. Carles. Critical nonlinear Schrödinger equations with and without harmonic potential. *arXiv:cond-math/0112414v4*, 2002.

[12] R. Carles. Remarks on Nonlinear Schrödinger Equations with Harmonic Potential. *Ann. Henri Poincaré*, 3:757, 2002.

[13] R. Carles. Nonlinear Schrödinger equations with repulsive harmonic potential and applications. *SIAM, J. Math. Analysis*, 35:823, 2003.

[14] T. Cazenave and F. B. Weissler. Rapidly Decaying Solutions of the Nonlinear Schrödinger Equation. *Commun. Math. Phys.*, 147:75, 1992.

[15] M. M. Cerimele, M. L. Chiofalo, F Pistella, S. Succi, and M. P. Tosi. Numerical solution of the Gross-Pitaevskii equation using an explicit finite-difference scheme: An application to trapped Bose-Einstein condensates. *Phys. Review E*, 62:1382, 2000.

[16] K. B. Davis, M. O. Mewes, M. R. Andrews, N. J. van Druten, D. S. Durfee, D. M. Kurn, and W. Ketterle. Bose-Einstein Condensation in a Gas of Sodium Atoms. *Phys. Review Lett.*, 75:3969, 1995.

[17] M. Edwards and K. Burenett. Numerical solution of the nonlinear Schrödinger equation for small samples of trapped neutral atoms. *Phys. Review A*, 51:1382, 1995.

[18] P. Gérard. The Cauchy problem for the Gross-Pitaevskii equation. *Ann. I.H.P., Anal. Nonlin.*, 23:765, 2006.

[19] J. Ginibre and G. Velo. On a Class of Nonlinear Schrödinger Equations. 1. The Cauchy Problem, General Case. *J. Functional Analysis*, 32:1, 1979.

[20] J. Ginibre and G. Velo. On a Class of Nonlinear Schrödinger Equations. 2. Scattering Theory, General Case. *J. Functional Analysis*, 32:33, 1979.

[21] J. Ginibre and G. Velo. On the global Chauchy problem for some non linear Schrödinger equations. *Ann. I.H.P., section C*, 1:309, 1984.

[22] J. Ginibre, G. Velo, and T. Ozawa. On the existence of the wave operators for a class of nonlinear Schrödinger equations. *Ann. I.H.P., section A*, 60:211, 1994.

[23] W. Hänsel, P. Hommelhoff, T. W. Hänsch, and J. Reichel. Bose-Einstein condensation on a microelectronic chip. *Nature*, 413:498, 2001.

[24] S. Hofferberth. *Coherent manipulation of Bose-Einstein condensates with rf adiabatic potentials*. PhD thesis, University of Heidelberg, 2007.

[25] R. Kosloff and D. Kosloff. Absorbing Boundaries for Wave Propagation Problems. *J. Comp. Physics*, 6:363, 1986.

[26] I. Lesanovsky, T. Schumm, S. Hofferberth, L. M. Andersson, P. Küger, and J. Schmiedmayer. Adiabatic radio-frequency potentials for coherent manipulation of matter waves. *Phys. Review A*, 73:033619, 2006.

[27] E. H. Lieb, R. Seiringer, and J. Yngvason. Bosons in a trap: A rigorous derivation of the Gross-Pitaevskii energy functional. *Phys. Review A*, 61:043602, 2000.

[28] H. Ott, J. Fortagh, G. Schlotterbeck, A. Grossmann, and C. Zimmermann. Bose-einstein condensation in a surface microtrap. *Phys. Review Lett.*, 87:230401, 2001.

[29] U. V. Riss and H. D. Meyer. Calculation of resonance energies and widths using the complex absorbing potential method. *J. Phys. B: At., Mol. and Opt. Phys.*, 26:4503, 1993.

[30] A. Sacchetti. Nonlinear time-dependent one-dimensional Schrödinger equation with double well potential. *J. Evolution Equations*, 4:345, 2002.

[31] L. Simon. Asymptotics for a class of nonlinear evolution equations with applications to geometric problems. *Ann. Math.*, 118:525, 1983.

[32] S. Succi, F. Toschi, M. P. Tosi, and P. Vignolo. Bose-Einstein Condensates and the numerical solution of the Gross-Pitaevskii equation. *Comp. Science and Engeneeing*, 7:48, 2005.

[33] X. Wen and N. J. Mauser. A new complex potential absorbing boundary layer for computing one dimensional nonlinear schrödinger equations, preprint.

[34] P. E. Zhidkov. The cauchy problem for a nonlinear Schrödinger equation, Dubna. *SIAM, J. Math. Analysis*, 1987.

CURRICULUM VITAE

Sofi Esterhazy

Geboren am 30.08.1983, Wien

Staatsbürgerschaft: Österreich

AUSBILDUNG:

Seit Juli 2008	Wissenschaftliche Mitarbeiterin am Wolfgang Pauli Institut (WPI)
Feb. – Sept. 2006	Auslandsemester an der Universität Jussieu, Paris (ERASMUS-Programm)
Nov. 2004	Abschluss des ersten Studienabschnitts
Nov. 2001 - April 2002	Volontariat im Entwicklungsprogramm der Organisation „ONE WORLD FOUNDATION“ in Ahungalla, Sri Lanka (6 Monate)
Seit Okt. 2001	Studium Mathematik-Diplom an der Universität Wien
Juni 2001	Reifeprüfung am GRG 19, Billrothstaße 73, Wien